

New fossils from Jebel Irhoud, Morocco and the pan-African origin of *Homo sapiens*

Jean-Jacques Hublin^{1,2}, Abdelouahed Ben-Ncer³, Shara E. Bailey⁴, Sarah E. Freidline¹, Simon Neubauer¹, Matthew M. Skinner⁵, Inga Bergmann¹, Adeline Le Cabec¹, Stefano Benazzi⁶, Katerina Harvati⁷ & Philipp Gunz¹

Fossil evidence points to an African origin of *Homo sapiens* from a group called either *H. heidelbergensis* or *H. rhodesiensis*. However, the exact place and time of emergence of *H. sapiens* remain obscure because the fossil record is scarce and the chronological age of many key specimens remains uncertain. In particular, it is unclear whether the present day ‘modern’ morphology rapidly emerged approximately 200 thousand years ago (ka) among earlier representatives of *H. sapiens*¹ or evolved gradually over the last 400 thousand years². Here we report newly discovered human fossils from Jebel Irhoud, Morocco, and interpret the affinities of the hominins from this site with other archaic and recent human groups. We identified a mosaic of features including facial, mandibular and dental morphology that aligns the Jebel Irhoud material with early or recent anatomically modern humans and more primitive neurocranial and endocranial morphology. In combination with an age of 315 ± 34 thousand years (as determined by thermoluminescence dating)³, this evidence makes Jebel Irhoud the oldest and richest African Middle Stone Age hominin site that documents early stages of the *H. sapiens* clade in which key features of modern morphology were established. Furthermore, it shows that the evolutionary processes behind the emergence of *H. sapiens* involved the whole African continent.

In 1960, mining operations in the Jebel Irhoud massif 55 km south-east of Safi, Morocco exposed a Palaeolithic site in the Pleistocene filling of a karstic network. An almost complete skull (Irhoud 1) was accidentally unearthed in 1961, prompting excavations that yielded an adult braincase (Irhoud 2)⁴, an immature mandible (Irhoud 3)⁵, an immature humeral shaft⁶, an immature ilium⁷ and a fragment of a mandible⁸, associated with abundant faunal remains and Levallois stone-tool technology⁶. Although these human remains were all reported to come from the bottom of the archaeological deposits, only the precise location of the humeral shaft was recorded.

The interpretation of the Irhoud hominins has long been complicated by persistent uncertainties surrounding their geological age. They were initially considered to be around 40 thousand years (kyr) old and an African form of Neanderthals⁹. However, these affinities have been challenged^{5,10,11} and the faunal⁸ and microfaunal¹² evidence supported a Middle Pleistocene age for the site. An attempt to date one of the hominins directly by uranium series combined with electron spin resonance (U-series/ESR)³ suggested an age of 160 ± 16 kyr (ref. 13). Consistent with some genetic evidence¹⁴, fossils from Ethiopia (Omo Kibish is considered to be as old as approximately 195 kyr (ref. 15) and Herto has been dated to approximately 160 thousand years ago (ka)¹⁶ are commonly regarded as the first early anatomically modern humans (EMH). Notably, Omo Kibish 1 and the Herto specimens appear to be more derived than the supposedly contemporaneous or even younger Irhoud hominins. It has therefore been suggested that the archaic features of the Irhoud fossils may indicate that north African *H. sapiens*

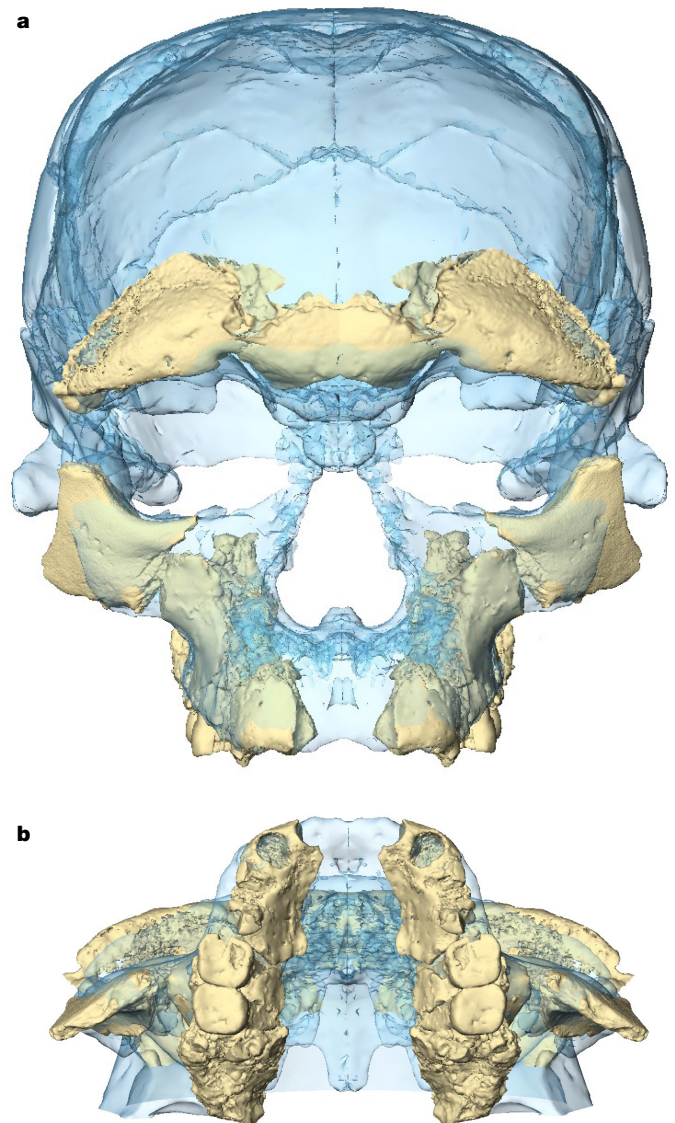


Figure 1 | Facial reconstruction of Irhoud 10. a, b, Frontal (a) and basal (b) views. This superimposition of Irhoud 10 (beige) and Irhoud 1 (light blue) represents one possible alignment of the facial bones of Irhoud 10. Nine alternative reconstructions were included in the statistical shape analysis of the face (see Methods and Fig. 3). The maxilla, zygomatic bone and supra-orbital area of Irhoud 10 are more robust than for Irhoud 1. Scale bar, 20 mm.

¹Department of Human Evolution, Max Planck Institute for Evolutionary Anthropology, Deutscher Platz 6, Leipzig 04103, Germany. ²Chaire Internationale de Paléanthropologie, Collège de France, Paris, France. ³Institut National des Sciences de l'Archéologie et du Patrimoine, Rabat, Morocco. ⁴Department of Anthropology, Center for the Study of Human Origins, New York University, New York, New York 10003, USA. ⁵School of Anthropology and Conservation, University of Kent, Canterbury CT2 7NR, UK. ⁶Department of Cultural Heritage, University of Bologna, Ravenna 48121, Italy. ⁷Paleoanthropology, Senckenberg Center for Human Evolution and Paleoenvironment, and DFG Center for Advanced Studies: “Words, Bones, Genes, Tools”, Eberhard Karls Universität, Tübingen, Germany.

interbred with Neanderthals¹⁷, or that the Irhoud hominins represented a north African, late surviving, archaic population¹⁸.

New excavations at Irhoud have enabled the recovery of *in situ* archaeological material and the establishment of a precise chronology of the deposits, which are much older than previously thought³. The excavation yielded a new series of hominin remains, including an adult skull (Irhoud 10) comprising a distorted braincase and fragments of the face (Fig. 1), a nearly complete adult mandible (Irhoud 11) (Fig. 2), one maxilla, several postcranial elements and abundant dental material (Extended Data Table 1). These remains primarily come from a single bone bed in the lower part of the archaeological deposits. This concentration, stratigraphic observations made by previous excavators and the anatomical similarity with earlier discoveries strongly suggest that most, if not all, of the hominin remains from the site were accumulated in a rather constrained window of time corresponding to the formation of layer 7. This layer contains the remains of at least five individuals (three adults, one adolescent and one immature individual, around 7.5 years old). The age of the site was redated to 315 ± 34 kyr (as determined by thermoluminescence dating)³, consistent with a series of newly established U-series/ESR dates, which places the Irhoud evidence in an entirely new perspective.

When compared to the large, robust and prognathic faces of the Neanderthals or older Middle Pleistocene forms, the facial morphologies of EMH and recent modern humans (RMH) are very distinctive. The face is relatively short and retracted under the braincase. Facial structures are coronally oriented and the infraorbital area is an ‘inflexion’ type, displaying curvatures along the horizontal, sagittal and coronal profiles. This pattern, which may include some primitive retentions¹⁹, strongly influences the morphology of the maxilla and zygomatic bone. Our morphometric analysis (Fig. 3 and Methods) clearly distinguishes archaic Middle Pleistocene humans and Neanderthals from RMH. By contrast, all the possible reconstructions of the new facial remains of Irhoud 10 fall well within RMH variation, as does Irhoud 1.

Another facial characteristic observed in RMH is the weakness of their brow ridges. Some EMH from Africa and the Levant still have protruding supraorbital structures, but they tend to be dissociated into a medial superciliary arch and a lateral supraorbital arch. Among the Irhoud hominins these structures are rather variable and this variability may be related to sexual dimorphism. Irhoud 1 has protruding supraorbital structures and the arches are poorly separated. However, in frontal view, the supraorbital buttress tends to form an inverted V above each orbit. On Irhoud 2, the torus is less projecting and a modern pattern can already be seen, with a clear sulcus separating the two arches. On Irhoud 10, the preserved parts do not show projecting supraorbital structures (Fig. 1). The new Irhoud 11 mandible is very large overall (Fig. 2 and Extended Data Table 2). As in some EMH from the Levant or north Africa, it has retained a vertical symphysis, with a mental angle of 88.8° (Extended Data Fig. 1). The mandibular body has a pattern typical of *H. sapiens*: its height strongly decreases from the front to the back. This feature is also present in the immature individual, Irhoud 3. Another modern aspect of Irhoud 11 is the rather narrow section of the mandibular body expressed by the breadth/height index at the level of the mental foramen (Extended Data Fig. 1). The Irhoud mandibles also show some derived conditions in the mental area (Extended Data Fig. 1). The symphyseal section of Irhoud 11 has a tear-shaped outline quite distinctive of *H. sapiens*. Although the Irhoud mandibles lack a marked mandibular incurvation, the juvenile Irhoud 3 has a central keel between two depressions expanding inferiorly into a thickened triangular eminence. This inverted T-shape, typical of recent *H. sapiens*²⁰, is incipient in the adult. Its inferior border is somewhat distended and includes separated tubercles. Notably, this modern pattern is still inconsistently present in Levantine EMH²⁰. In some aspects, Irhoud 11 is evocative of the Tabun C2 mandible, but it is much more robust.

The Irhoud teeth are generally very large (Extended Data Tables 3, 4). However, their dental morphology is reminiscent of EMH in several

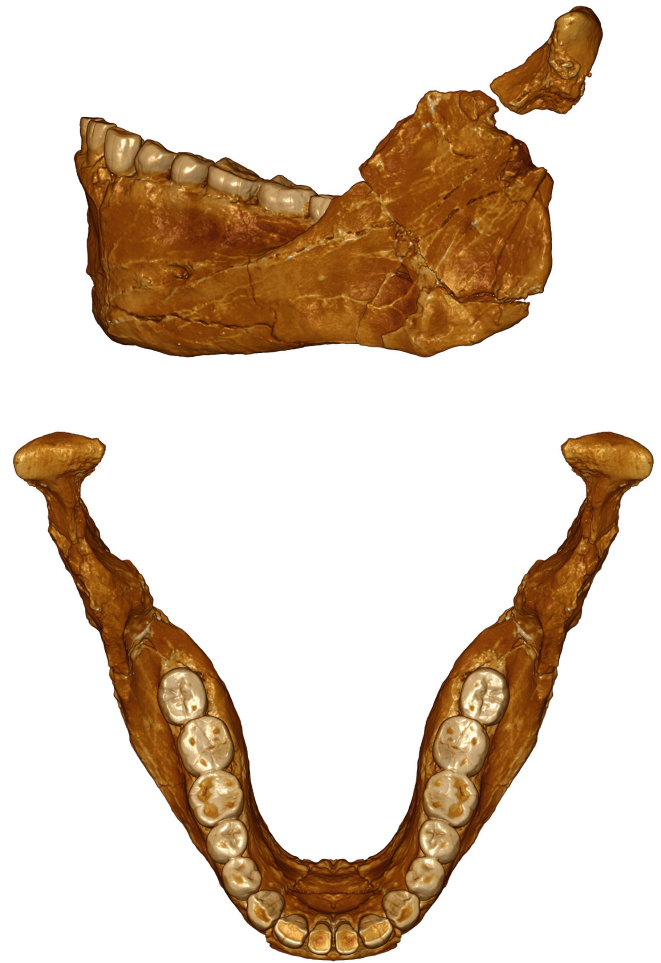


Figure 2 | Irhoud 11 mandible (lateral and occlusal views). See Methods for the reconstruction. The bi-condylar breadth of the Irhoud 11 mandible fits the width of the corresponding areas on the Irhoud 2 skull exactly. Scale bar, 20 mm.

respects. The anterior teeth do not display the expansion observed in non-*sapiens* Middle Pleistocene hominins and Neanderthals²¹ and the post-canine teeth are reduced compared to older hominins. The third maxillary molar (M^3) of Irhoud 21 is already smaller than in some EMH. The crown morphology (Extended Data Table 5 and Extended Data Fig. 2) also aligns the Irhoud specimens most closely with *H. sapiens*, rather than with non-*sapiens* Middle Pleistocene hominins and Neanderthals. They do not display expanded and protruding first upper molar (M^1) hypocones, lower molar middle trigonid crests (especially at the enamel–dentine junction (EDJ)), or a second lower premolar (P_4) with a transverse crest, uninterrupted by a longitudinal fissure. The molars are morphologically complex and similar to the large teeth of African EMH, possessing accessory features such as a cusp 6, cusp 7 and protostylid on the lower molars and cusp 5 on the upper molars. The EDJ analysis demonstrates the retention of a non-Neanderthal primitive pattern of the P_4 (Extended Data Fig. 2b). However, derived crown shapes shared with RMH are already seen in the upper and lower molars, grouping Irhoud 11 with EMH from north Africa and the Levant. The lower incisor and canine roots retain a large size, but the shape is already within the range of the modern distribution (Extended Data Fig. 3). Mandibular molar roots are cynodont, that is, modern-human-like. This mandibular root configuration of Irhoud 11 is similar to that observed in EMH from Qafzeh. Finally, Irhoud 3 shows a pattern of eruption and a period of dental development close to recent *H. sapiens*¹³.

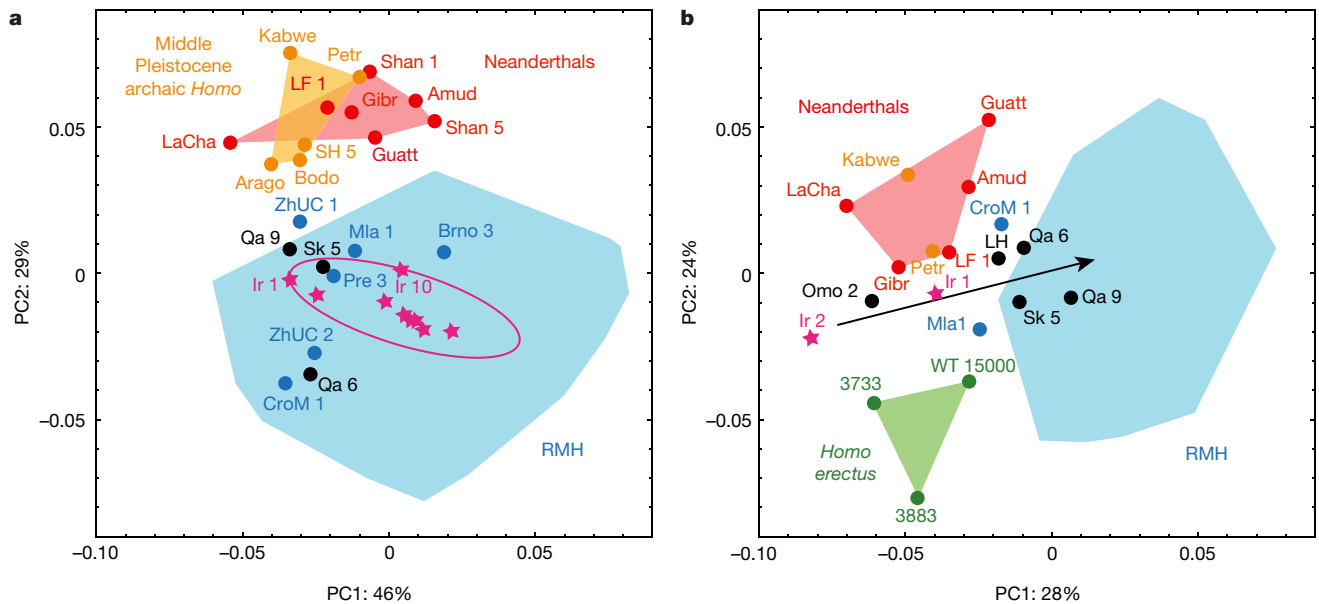


Figure 3 | Comparative shape analysis. **a**, Principal component analysis (PCA) of the facial shape. EMH (black) and RMH (blue) are well separated from Neanderthals and archaic Middle Pleistocene hominins. Irhoud (Ir 1) and all nine alternative reconstructions of Irhoud 10 (pink stars and pink 99% confidence ellipse, see Methods) fall within the RMH variation. **b**, PCA of the endocranial shape. RMH (blue), Neanderthals

(red) and *Homo erectus* (green) are separated. Archaic Middle Pleistocene hominins (orange) plot with Neanderthals. Irhoud 1 and 2 (pink stars) and some EMH (black) fall outside the RMH variation. Shape differences are visualized in Extended Data Fig. 5a. Sample compositions and abbreviations can be found in the Methods.

In contrast to their modern facial morphology, the Irhoud crania retain a primitive overall shape of the braincase and endocranial shape, that is, unlike those of RMH, they are elongated and not globular^{10,18,22}. This results in a low outline of the occipital squama, elongated temporal bones and a low convexity of the parietal¹¹. However, the frontal squama has a vertical orientation and a marked convexity when compared to archaic Middle Pleistocene specimens. These derived conditions are especially well expressed on Irhoud 2 (ref. 11). A geometric morphometric analysis (Extended Data Fig. 4) of external vault shape distinguishes Neanderthals and archaic Middle Pleistocene forms with their primitive neurocranial shape from RMH and Upper Palaeolithic humans. With regards to the first principal component (PC)1, Irhoud 1 and 2 are intermediate and group together with specimens such as Laetoli H18 and Qafzeh, as well as Upper Palaeolithic individuals from Mladeč or Zhoukoudian Upper Cave. To some degree all of these specimens retained longer and lower braincase proportions compared to RMH. The morphometric analysis of endocranial shape (Fig. 3b), which is not affected by cranial superstructures, shows a clear separation between *H. erectus* and the Neanderthal/archaic Middle Pleistocene cluster along PC2. The latter have evolved larger neocortices but, in contrast to RMH, without a proportional increase in the cerebellum (Extended Data Fig. 5). EMH and the Irhoud hominins also display elongated endocranial profiles, but are intermediate between *H. erectus* and the cluster of Neanderthals/archaic Middle Pleistocene hominins along PC2. They range in rough agreement with their geological age along PC1, in a morphological cline ending with the extant globular brain shapes of RMH. Notably, Omo Kibish 2 falls between Irhoud 1 and 2. This similarity continues the question of the contemporaneity of Omo Kibish 1 and 2, two specimens with very different braincase morphologies²³.

The Irhoud fossils currently represent, to our knowledge, the most securely dated evidence of the early phase of *H. sapiens* evolution in Africa, and they do not simply appear as intermediate between African archaic Middle Pleistocene forms and RMH. Even approximately 300 ka ago their facial morphology is almost indistinguishable from that of RMH, corroborating the interpretation of the fragmentary specimen from Florisbad (South Africa) as a primitive

H. sapiens tentatively dated to 260 ka (ref. 24). Mandibular and dental morphology, as well as the pattern of dental development also align the Irhoud fossils with EMH. Notably, the endocranial analysis suggests diverging evolutionary trajectories between early *H. sapiens* and African archaic Middle Pleistocene forms. This anatomical evidence and the chronological proximity between these two groups²⁵ reinforce the hypothesis of a rapid anatomical shift or even, as suggested by some²⁶, of a chronological overlap. The Irhoud evidence supports a complex evolutionary history of *H. sapiens* involving the whole African continent^{25,27}. Like in the Neanderthal lineage²⁸, facial morphology was established early on, and evolution in the last 300 ka primarily affected the braincase. This occurred together with a series of genetic changes affecting brain connectivity²⁹, organization and development²². Through accretional changes, the Irhoud morphology is directly evolvable into that of extant humans. Delimiting clear-cut anatomical boundaries for a 'modern' grade within the *H. sapiens* clade thus only depends on gaps in the fossil record³⁰.

Online Content Methods, along with any additional Extended Data display items and Source Data, are available in the online version of the paper; references unique to these sections appear only in the online paper.

Received 4 May 2016; accepted 6 April 2017.

1. Stringer, C. Modern human origins: progress and prospects. *Phil. Trans. R. Soc. B* **357**, 563–579 (2002).
2. Bräuer, G. The origin of modern anatomy: by speciation or intraspecific evolution? *Evol. Anthropol.* **17**, 22–37 (2008).
3. Richter, D. et al. The age of the Jebel Irhoud (Morocco) hominins and the origins of the Middle Stone Age. *Nature* <http://dx.doi.org/10.1038/nature22335> (2017).
4. Ennouchi, E. Le deuxième crâne de l'homme d'Irhoud. *Annales de Paléontologie (Vérrébrés)* **LIV**, 117–128 (1968).
5. Hublin, J.-J. & Tillier, A. M. in *Aspects of Human Evolution Vol. 21 Symposia of the Society for the study of Human Biology, Volume XXI* (ed. Stringer, C. B.) 167–186 (Taylor & Francis, 1981).
6. Hublin, J.-J., Tillier, A. M. & Tixier, J. L'humérus d'enfant moustérien (Homo 4) du Jebel Irhoud (Maroc) dans son contexte archéologique. *Bull. Mem. Soc. Anthropol. Paris* **4**, 115–141 (1987).
7. Tixier, J., Brugal, J.-P., Tillier, A.-M., Bruzeket, J. & Hublin, J.-J. in *Actes des 1ères Journées Nationales d'Archéologie et du Patrimoine. Préhistoire Vol. 1* 149–153 (Société Marocaine d'Archéologie et du Patrimoine, 2001).

8. Amani, F. & Geraads, D. Le gisement moustérien du Jebel Irhoud, Maroc: précisions sur la faune et la biochronologie, et description d'un nouveau reste humain. *Comptes Rendus à l'Académie des Sciences de Paris* **316**, 847–852 (1993).
9. Ennouchi, E. Un Néanderthalien: l'homme du Jebel Irhoud (Maroc). *Anthropologie* **66**, 279–299 (1962).
10. Stringer, C. B in *Recent advances in Primatology*. (eds Chivers, D. J. & Joysey, K. A.) 395–418 (Academic, 1978).
11. Hublin, J.-J. Recent human evolution in northwestern Africa. *Phil. Trans. R. Soc. B* **337**, 185–191 (1992).
12. Geraads, D. et al. The rodents from the late middle Pleistocene hominid-bearing site of J'bel Irhoud, Morocco, and their chronological and paleoenvironmental implications. *Quat. Res.* **80**, 552–561 (2013).
13. Smith, T. M. et al. Earliest evidence of modern human life history in North African early *Homo sapiens*. *Proc. Natl Acad. Sci. USA* **104**, 6128–6133 (2007).
14. Gonder, M. K., Mortensen, H. M., Reed, F. A., de Sousa, A. & Tishkoff, S. A. Whole-mtDNA genome sequence analysis of ancient African lineages. *Mol. Biol. Evol.* **24**, 757–768 (2007).
15. McDougall, I., Brown, F. H. & Fleagle, J. G. Stratigraphic placement and age of modern humans from Kibish, Ethiopia. *Nature* **433**, 733–736 (2005).
16. White, T. D. et al. Pleistocene *Homo sapiens* from Middle Awash, Ethiopia. *Nature* **423**, 742–747 (2003).
17. Smith, F. H. in *Continuity or Replacement, Controversies in Homo sapiens evolution* (eds Bräuer, G. & Smith, F. H.) 145–156 (A. A. Balkema, Zagreb, 1992).
18. Bruner, E. & Pearson, O. Neurocranial evolution in modern humans: the case of Jebel Irhoud 1. *Anthropol. Sci.* **121**, 31–41 (2013).
19. Bermúdez de Castro, J. M. & Martínón-Torres, M. Evolutionary interpretation of the modern human-like facial morphology of the Atapuerca Gran Dolina-TD6 hominins. *Anthropol. Sci.* **122**, 149–155 (2014).
20. Schwartz, J. H. & Tattersall, I. The human chin revisited: what is it and who has it? *J. Hum. Evol.* **38**, 367–409 (2000).
21. Trinkaus, E. Dental remains from the Shanidar adult Neanderthals. *J. Hum. Evol.* **7**, 369–382 (1978).
22. Gunz, P. et al. A uniquely modern human pattern of endocranial development. Insights from a new cranial reconstruction of the Neandertal newborn from Mezmaiskaya. *J. Hum. Evol.* **62**, 300–313 (2012).
23. Klein, R. G. *The Human Career: Human Biological and Cultural Origins* 3rd edn (Chicago Univ. Press, 2009).
24. Grün, R. et al. Direct dating of Florisbad hominid. *Nature* **382**, 500–501 (1996).
25. Stringer, C. *The Origin of Our Species*. (Allen Lane, Penguin, 2011).
26. Harvati, K. et al. The later Stone Age calvaria from Iwo Eleru, Nigeria: morphology and chronology. *PLoS ONE* **6**, e24024 (2011).
27. Gunz, P. et al. Early modern human diversity suggests subdivided population structure and a complex out-of-Africa scenario. *Proc. Natl Acad. Sci. USA* **106**, 6094–6098 (2009).
28. Arsuaga, J. L. et al. Neandertal roots: cranial and chronological evidence from Sima de los Huesos. *Science* **344**, 1358–1363 (2014).
29. Meyer, M. et al. A high-coverage genome sequence from an archaic Denisovan individual. *Science* **338**, 222–226 (2012).
30. Weaver, T. D. Did a discrete event 200,000–100,000 years ago produce modern humans? *J. Hum. Evol.* **63**, 121–126 (2012).

Acknowledgements The research program at Jebel Irhoud is jointly conducted and supported by the Moroccan Institut National des Sciences de l'Archéologie et du Patrimoine and the Department of Human Evolution of the Max Planck Institute for Evolutionary Anthropology. We are grateful to the many curators and colleagues who, over the years, gave us access to recent and fossil hominin specimens for computed tomography scanning or analysis, to E. Trinkaus for providing comparative data and to C. Kiarie, M. Lui, C. Piot, D. Plotzki, A. Buchenau and H. Temming for their technical assistance.

Author Contributions The study was conceived by J.-J.H., A.B.-N. and P.G. Cranial metrical and non-metrical data were compiled and analysed by J.-J.H., A.B.-N., S.E.F., S.N., K.H. and P.G. Mandibular metrical and non-metrical data were compiled and analysed by J.-J.H. and I.B. Dental metrical and non-metrical data were compiled and analysed by S.E.B., M.M.S., A.L.C. and S.B. J.-J.H. and P.G. wrote the manuscript with contributions from all other authors.

Author Information Reprints and permissions information is available at www.nature.com/reprints. The authors declare no competing financial interests. Readers are welcome to comment on the online version of the paper. Publisher's note: Springer Nature remains neutral with regard to jurisdictional claims in published maps and institutional affiliations. Correspondence and requests for materials should be addressed to J.-J.H. (hublin@eva.mpg.de) or P.G. (gunz@eva.mpg.de).

Reviewer Information *Nature* thanks R. G. Klein, C. Stringer and the other anonymous reviewer(s) for their contribution to the peer review of this work.

METHODS

Data reporting. No statistical methods were used to predetermine sample size. The experiments were not randomized and the investigators were not blinded to allocation during experiments and outcome assessment.

Computed tomography. The original fossil specimens were scanned using a BIR ARCTIS 225/300 industrial micro-computed tomography scanner, at the Max Planck Institute for Evolutionary Anthropology (MPI EVA), Leipzig, Germany. The non-dental material was scanned with an isotropic voxel size ranging from 27.4 to 91.4 μm (130 kV, 100–150 μA , 0.25–2.0 mm brass filter, 0.144° rotation steps, 2–3 frames averaging, 360° rotation). The dental material was scanned with an isotropic voxel size ranging from 12.8 to 32.8 μm (130 kV, 100 μA , 0.25–0.5 mm brass filter, 0.144° rotation steps, 3 frames averaging, 360° rotation). Segmentation of the micro-computed tomography volume was performed in Avizo (Visualization Sciences Group). The comparative dental sample was scanned with an isotropic voxel size ranging from 11.6 to 39.1 μm at the MPI EVA on a BIR ARCTIS 225/300 micro-computed tomography scanner (130–180 kV, 100–150 μA , 0.25–2.0 mm brass filter, 0.096–0.144° rotation steps, 2–4 frames averaging, 360° rotation) or on a Skyscan 1172 micro-computed tomography scanner (100 kV, 100 μA , 0.5 mm aluminium and 0.04 mm copper filters, 0.10–1.24° rotation steps, 360° rotation, 2–4 frames averaging). The micro-computed tomography slices were filtered using a median filter followed by a mean-of-least-variance filter (each with a kernel size of three) to reduce the background noise while preserving and enhancing edges³¹.

Virtual reconstruction. Using Avizo, nine reconstructions of the Jebel Irhoud 10 face were made on the basis of the segmented surfaces of its preserved parts consisting of a left supraorbital torus, two left maxillary fragments and a nearly complete left zygomatic bone. First, we used several RMH from diverse geographical regions (for example, Africa, North America and Australia) and Irhoud 1 as a reference to align the two left maxillary bones. Since a large portion of the dental arcade of Irhoud 10 is preserved, the range of possible ‘anatomically correct’ alignments in the palate was limited (Fig. 1b). On the basis of this maxillary alignment, each of the subsequent reconstructions differed by several millimetres in the following ways: broadening the palate; increasing the facial height; increasing the orbital height; or rotating the zygomatic bones anteriorly or posteriorly in a parasagittal direction. Additionally, we aligned one reconstruction to match the facial proportions and orientation of a ‘classic’ Neanderthal (La Ferrassie 1). In doing so, the zygomatic bone was rotated parasagittally and moved posteriorly (>5 mm). Correspondingly, the brow ridge was realigned postero-superiorly by several mm, and the maxillary bones were moved inferiorly by several mm to increase its facial height. For each reconstruction, each bone was mirror-imaged along the midsagittal plane of Irhoud 1 and then the right and left sides were merged to form one surface model. The reconstruction of the Irhoud 11 mandible was conducted by mirroring the left side of the mandible, which was best preserved and minimally distorted, onto the right side, apart from the condyle, which was only preserved on the right side and mirrored onto the left side. The left side of the mandible was represented by three main fragments. Before mirroring, the sediment filling the cracks between the main fragments was virtually removed, the fragments were re-fitted and the broken crown of the left canine was reset on its root. Note that the position of the condyles in the reconstruction is only indicative.

Shape analysis of the face, endocast and cranial vault. Geometric morphometric methods (GMM) were used to analyse different aspects of the morphology of the Irhoud fossils in a comparative context. To this end we digitized 3D landmarks and sliding semilandmarks^{32–34} to separately analyse the shape of the face, the endocranial profile and the external vault. On the face (Fig. 3a), 3D coordinates of anatomical landmarks, as well as the curve and surface semilandmarks ($n = 791$) were digitized using Landmark Editor³⁵ either on computed tomography scans (BIR ACTIS 225/300 and Toshiba Aquilion), or surface scans (Minolta Vivid 910 and Breuckmann optoTOP-HE) of recent modern human and fossil crania ($n = 267$) following previously published protocols³⁶. Whenever possible, measurements were taken on scans of the original fossil; landmarks on some fossil specimens were measured on scans of research-quality casts. Avizo was used to extract surface files from the computed tomography scans; data from surface scanners were pre-processed using Geomagic Studio (Geomagic Inc.) and OptoCat (Breuckmann).

On the endocast (Fig. 3b), landmarks and semilandmarks ($n = 31$) along the internal midsagittal profile of the braincase were digitized on computed tomography scans of the original specimens ($n = 86$) in Avizo (Visualization Sciences Group) following the measurement protocol described in ref. 37, and converted to 2D data by projecting them onto a least squares plane in Mathematica (Wolfram Research).

On the external vault (Extended Data Fig. 4), coordinate measurements of 97 anatomical landmarks and curve semilandmarks (along the external midsagittal profile from glabella to inion, the coronal and lambdoid sutures, and along the upper margin of the supraorbital torus) were captured using a Microscribe 3DX

(Immersion Corp.) portable digitizer on recent and fossil braincases ($n = 296$) following the measurement protocol described in ref. 38. The points along sutures were later resampled automatically in Mathematica to ensure the same semilandmark count on every specimen.

H. erectus samples include KNM ER 3733 (3733), KNM ER 3883 (3883), KNM WT 15000. Archaic Middle Pleistocene samples include Petralona (Petr), Arago, Sima de los Huesos H5 (SH5), Saldanha, Kabwe, Bodo. Neanderthal samples include La Chapelle-aux-Saints 1 (LaCha), Guattari 1 (Guatt), La Ferrassie 1 (LF 1), Forbes’ Quarry 1 (Gibr), Feldhofer (Feld), La Quina 5 (LQ 5), Spy 1 and 2 (Sp 1 and Sp 2), Amud 1 (Amud), Shanidar 1 and 5 (Shan 1 and Shan 5). Primitive *H. sapiens* and EMH specimens include Laetoli H18 (LH), Omo Kibish 2 (Omo 2), Singa (Si), Qafzeh 6 and 9 (Qa 6 and Qa 9), Skhul 5 (Sk 5). Upper Palaeolithic modern human specimens include Cro-Magnon 1 and 3 (CroM 1 and CroM 3), Mladeč 1 and 5 (Mla 1 and Mla 5), Brno 3, Předmostí 3 and 4 (Pre 3 and Pre 4), Abri Pataud (AbP), Cioclovina (Ci), Zhoukoudian Upper Cave 1 and 2 (ZhUC 1 and ZhUC 2). The RMH samples are composed of individuals of diverse geographical origins ($n = 232$ individuals in Fig. 3a, $n = 55$ individuals in Fig. 3b, $n = 263$ individuals in Extended Data Fig. 4).

Crown outline analysis. The crown outline analysis (Extended Data Fig. 3a) of Irhoud 10 and Irhoud 21 left M¹ follows previously described protocols^{39,40}. For Irhoud 10, computed tomography images were virtually segmented using a semi-automatic threshold-based approach in Avizo to reconstruct a 3D digital model of the tooth, which was then imported in Rapidform XOR2 (INUS Technology, Inc.) to compute the cervical plane. The tooth was aligned with the cervical plane parallel to the x - y plane of the Cartesian coordinate system and rotated around the z axis with the lingual side parallel to the x axis. The crown outline corresponds to the silhouette of the oriented crown as seen in occlusal view and projected onto the cervical plane. For Irhoud 21, an occlusal image of the crown was taken with a Nikon D700 digital camera and a Micro-Nikkor 60 mm lens. The tooth was oriented so that the cervical border was perpendicular to the optical axis of the camera lens. The image was imported into the Rhino 4.0 Beta CAD environment (Robert McNeel & Associates) and aligned to the x - y plane of the Cartesian coordinate system. The crown outline was digitized manually using the spline function, and then oriented with the lingual side parallel to the x axis. Both crown outlines⁴¹ were first centred superimposing the centroids of their area according to the M¹ sample from ref. 40, but combined with 10 additional late early and Middle Pleistocene *Homo* M¹ specimens (that is, Arago-31, AT-406, ATD6-11, ATD6-69, ATD6-103, Bilzingsleben-76-530, Petralona, Steinheim, Rabat, Thomas 3). Then, the outlines were represented by 24 pseudolandmarks obtained by equiangularly spaced radial vectors out of the centroid (the first radius is directed buccally and parallel to the y axis of the Cartesian coordinate system), and scaled to unit centroid size^{39,41}. Late Early and Middle Pleistocene archaic samples include Arago 31 (Ar 31), Atapuerca Gran Dolina 6-11, 6-69, 6-103 (ATD6-11, ATD6-69, ATD6-103), Atapuerca Sima de los Huesos 406 (AT-406), Bilzingsleben-76-530 (Bil76-530), Petralona (Petr), Steinheim (Stein), Rabat (Rab), Thomas 3 (Tho 3). The Neanderthal sample includes Arcy-sur-Cure 39, Cova Negra, Krapina (KDP 1, KDP 3, KDP 22, D101, D171, Max C, Max D), La Ferrassie 8, La Quina H18, Le Fate XIII, Le Moustier 1, Monsempron 1953-1, Obi Rakhmat, Petit Puymoyen, Roc de Marsal, Saint-Césaire 1. EMH specimens include Dar es-Soltan II-NN and II-H6 (DSII-NN and DSII-H6), Qafzeh 10 and 15 (Qa 10 and Qa 15), Skhul 1 (Skh 1), Contrebandiers H7 (CT H7). Upper Palaeolithic modern human samples include Abri Pataud, Fontéchevade, Gough’s Cave (Magdalenian), Grotta del Fossellone, Kostenki 15, Lagar Velho, Laugerie-Basse, La Madeleine, Les Rois 19, Les Rois unnumbered, Mladeč (1 and 2), Peskó Barlang, St Germain (2, B6, B7), Sungir (2, 3), Veyrier 1. The RMH samples are composed of individuals of diverse geographical origins ($n = 80$).

Molar and premolar EDJ shape analysis. Enamel and dentine tissues (Extended Data Fig. 3b) of lower second molars and second premolars were segmented using the 3D voxel value histogram and its distribution of greyscale values^{42,43}. After the segmentation the EDJ was reconstructed as a triangle-based surface model using Avizo (using unconstrained smoothing). Small EDJ defects were corrected digitally using the ‘fill holes’ module of Geomagic Studio. We then used Avizo to digitize 3D landmarks and curve-semilandmarks on these EDJ surfaces^{42,43}. For the molars, anatomical landmarks were placed on the tip of the dentine horn of the protoconid, metaconid, entoconid and hypoconid. For the premolars anatomical landmarks were placed on protoconid and metaconid dentine horns. Moreover, we placed a sequence of landmarks along the marginal ridge connecting the dentine horns beginning at the top of the protoconid moving in lingual direction; the points along this ridge curve were then later resampled to the same point count on every specimen using Mathematica. Likewise, we digitized and resampled a curve along the cemento-enamel junction as a closed curve starting and ending below the protoconid horn and the mesiobuccal corner of the cervix. The resampled points

along the two ridge curves were subsequently treated as sliding curve semilandmarks and analysed using GMM together with the four anatomical landmarks. *H. erectus* specimens includes KNM-ER 992 second lower molar and second lower premolar (M_2 and P_4), S1b (M_2 and P_4), S5, S6a. We also included the *H. habilis*⁴⁴ specimen KNM-ER-1802 to establish trait polarity. Archaic Middle Pleistocene samples include Mauer (M_2 and P_4), Balanica BH-1 (Bal) and KNM-BK 67. The Neanderthal sample includes Abri Suard S36, Combe Grenal (29, IV, VIII), El Sidron (303, 540, 755, 763a), Krapina (53, 54, 55, 57, 59, D1, D6, D9, D35, D50, D80, D86, D105, D107), La Quina H9, Le Moustier 1 (M_2 and P_4), Le Regourdou 1 (M_2 and P_4), Scladina I-4A (M_2 and P_4), Vindija 11-39. EMH samples include Dar es-Soltan II H4 (DS II-H4), El Harhoura (El H; M_2 and P_4), Irhoud 11 (Ir 11; M_2 and P_4), Irhoud 3 (Ir 3; M_2 and P_4), Qafzeh 9 (M_2 and P_4), Qafzeh 10, Qafzeh 11 (M_2 and P_4), Qafzeh 15, Contrebandiers 1 (CT; M_2 and P_4). The RMH samples are composed of individuals of diverse geographical origins (M_2 sample, $n=8$; P_4 sample, $n=8$).

Tooth root shape analysis. Analysis is shown in Extended Data Fig. 3. Dental tissues (enamel, dentine and pulp) of the anterior dentition were first segmented semiautomatically using a region growing tool, and when possible using the watershed principle⁴⁵; this segmentation was edited manually to correct for cracks. Each tooth was then virtually divided into crown and root by cutting the 3D models at the cervical plane defined by a least-square-fit plane between the landmarks set at the points of the greatest curvature on the labial and lingual sides of the cement–enamel junction. Following the protocol described in ref. 46, we analysed dental root shape: using Avizo, a landmark was digitized at the root apex and a sequence of 3D landmark coordinates was recorded along the cement–enamel junction. Using Mathematica, this curve was then resampled to 50 equidistant curve-semilandmarks. The shape of the root surface, delimited by the cervical semilandmarks and the apical landmark, was quantified using 499 surface-semilandmarks⁴⁶; a mesh of 499 landmarks was digitized manually on a template specimen, then warped to each specimen using a thin-plate spline interpolation and lofted onto the segmented root surface by projecting to closest surface vertex. These landmarks and semilandmarks were then analysed using GMM. *H. erectus* is represented by KNM-WT 15000 (WT 15000). The Neanderthal samples include Krapina (Krp53, Krp 54, Krp 55, Krp 58, Krp 59), Saint-Césaire 1 (SC), Abri Bourgeois-Delaunay 1 (BD1), Kebara 2 and 28 (Keb 2, KMH 28). EMH samples include Contrebandiers 1 (Tem) Qafzeh 8 and 9 (Qa 8, Qa 9) and Tabun C2 (Tab C2). Upper Palaeolithic and Mesolithic modern samples include individuals from Oberkassel (Ob), Nahal-Oren (NO 8, NO 14), Hayonim (Ha 8, Ha 19, Ha 20), Kebara (Keb A5) and Combe-Capelle (CC). The RMH samples include individuals of diverse geographical origins ($n=47$).

Statistical analysis. 3D landmark and semilandmark data were analysed using GMM functions in Mathematica^{34,47}. Curves and surfaces were quantified using sliding semilandmarks on the basis of minimizing the thin-plate spline bending energy³² between each specimen and the sample mean shape^{33,34}. Missing landmarks or semilandmarks were estimated using a thin-plate spline interpolation on the basis of the sample mean shape during the sliding process⁴⁸. After sliding, all landmarks and semilandmarks were converted to shape variables using generalized least-squares Procrustes superimposition⁴⁹; these data were then analysed using PCA, and between group PCA⁵⁰. For the M^1 crown outlines analysis, the shape variables of the outlines were projected into the shape–space obtained from a PCA of the comparative M^1 sample. The data were processed and analysed through software routines written in R⁵¹.

Mandibular metric data. Data are shown in (Extended Data Table 2 and Extended Data Fig. 1c). Linear measurements were taken on 3D surface models generated from micro-computed tomography data in Avizo. They were complemented by measurements of the original specimens taken by E. Trinkaus (Extended Data Fig. 1c) and by comparative data taken from the literature^{52–98}. The African and European archaic Middle Pleistocene samples include KNM-BK 67, KNM-BK 8518, Sidi Abderrahmane 2, Thomas Quarry I, Thomas Quarry Gh 10717, Tighenif (1, 2, 3), Arago (I, XIII), Mauer, Montmaurin 1, Sima de los Huesos (XIX, XXI, XXVIII), AT 1, AT 75, AT 300, AT 605, AT 607. The Asian Neanderthal specimens include Amud 1, Chagyrskaya 6, Kebara 2, Shanidar (1, 2, 4) and Tabun C1. The European Neanderthal specimens include Arcy II, Banyoles, El Sidrón (1, 2, 3), Guattari (2, 3), Hortus 4, Krapina (57, 58, 59), Suard S 36, Bourgeois Delaunay 1, La Ferrassie 1, La Quina 5, La Naulette 1, Le Regourdou 1, Saint-Césaire 1, Sima de las Palomas (1, 6, 23, 59), Spy (1, 3), Subalyuk 1, Vindija (206, 226, 231, 250, 11.39, 11.40, 11.45), Weimar-Ehringsdorf F1009 and Zafarraya. The EMH specimens include Dar es-Soltan II-H5, El Harhoura 1, Dire Dawa, Klasies River (KRM 13400, KRM 14695, KRM 16424, KRM 21776, KRM 41815), Qafzeh (9, 26, 27), Skhul (IV, V), Tabun C2 and Contrebandiers 1. The Upper Palaeolithic and Epipalaeolithic sample includes individuals from Abri Pataud 1, Arene Candide (2, 18), Asselar, Barma del Caviglione, Chancelade, Cro Magnon (1, 3), Dar es-Soltan (II-H2, II-H3), Dolni Věstonice (3, 13, 14, 15, 16), El Mirón, Grotte des Enfants 4, Hayonim (8, 17, 19, 20, 25, 27, 29 and 29a), Isturitz (106 and 115), Le Roc (1, 2), Minat 1, Moh

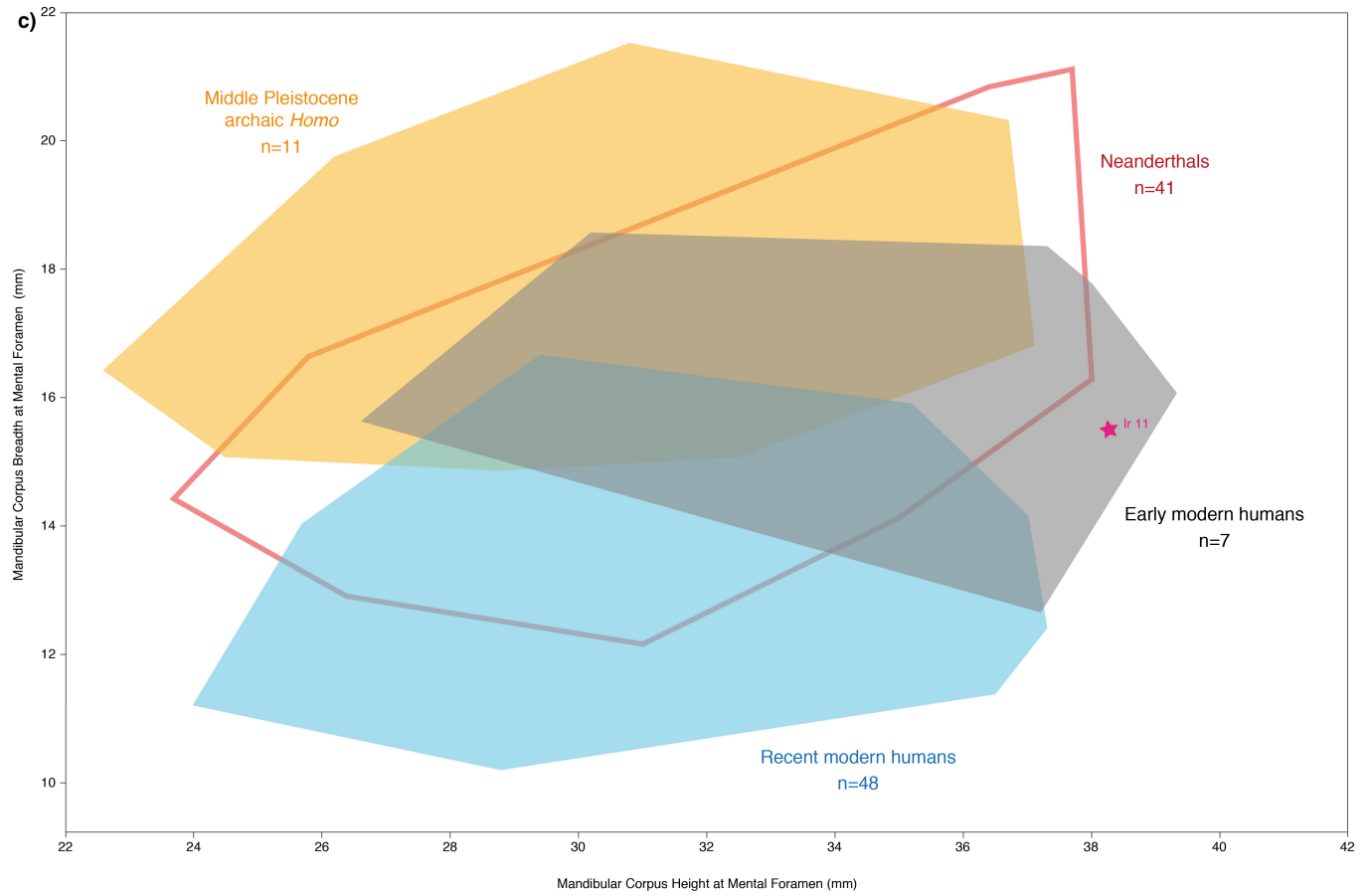
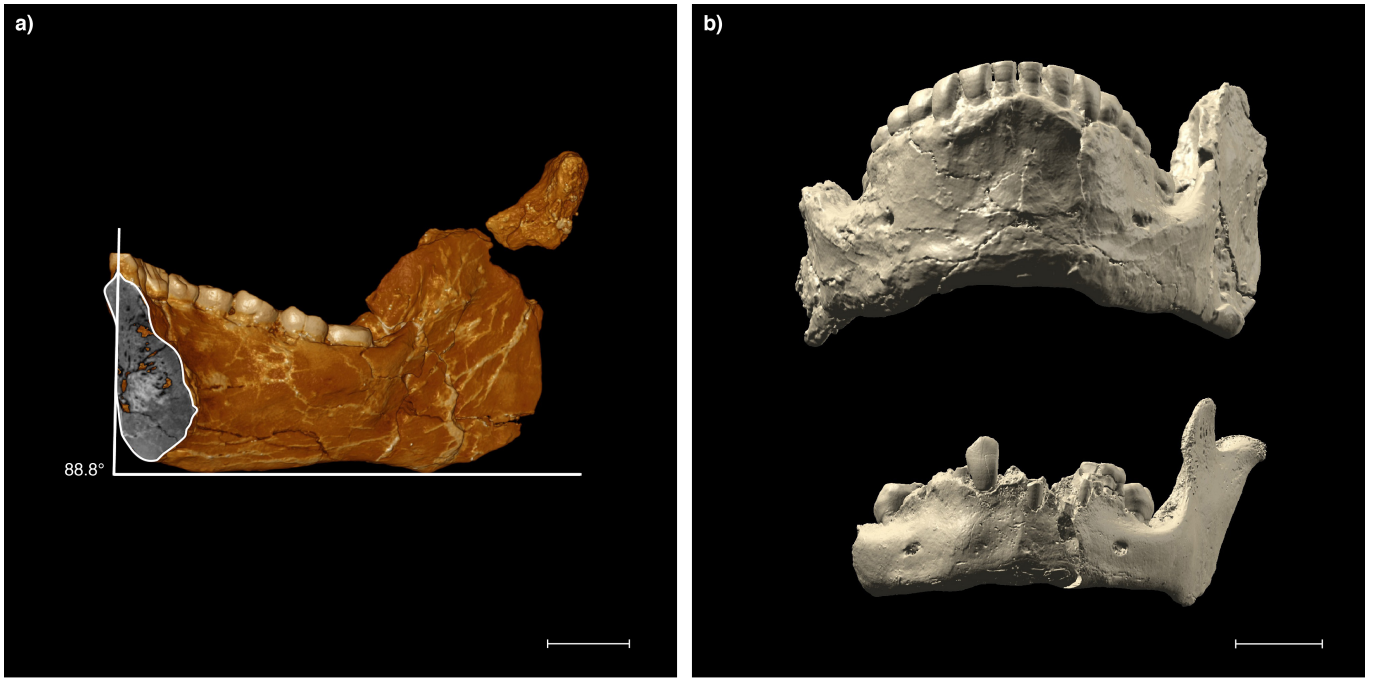
Khiew, Muierii 1, Nahal Oren (6, 8, 14, 18), Nazlet Khater 2, Oase 1, Oberkassel (1, 2), Ohalo II (1, 2), Pavlov 1, Předmostí (3, 21), Sunghir (1, 6), Villabruna 1 and Zhoukoudian Upper Cave (101, 104, 108).

Dental metric and non-metric data. Crown metric and non-metric data (Extended Data Fig. 3 and Extended Data Tables 3–5) were collected from casts or originals with a few exceptions taken from the literature. The latter include: Mumba XII (ref. 99), Eyasi¹⁰⁰, Kaphthurin¹⁰¹, Olduvai¹⁰², Sima de los Huesos¹⁰³ and some Sangiran metric data¹⁰⁴. Root metric data were taken on 3D models generated from micro-computed tomographic data¹⁰⁵. Crown measurements were taken using Mitutoyo digital callipers. Non-metric trait expressions were scored using the Arizona State University Dental Anthropology System¹⁰⁶ where applicable (for lower dentition: P_4 lingual cusps, cusp 6, cusp 7, M groove pattern, protostylid; for upper dentition: shovelling, tuberculum dentale, canine distal accessory ridge, cusp 5, Carabelli's trait, parastyle, metacone and hypocone reduction), and ref. 107 for all others. The RMH sample includes individuals from south, west and east Africa, western and central Europe, northeast Asia, west Asia, India, Australia, New Guinea and Andaman Islands. For root metrics (Extended Data Fig. 3) the sample composition can be found in table 1 of ref. 105. In Extended Data Tables 3–5, *H. erectus* includes individuals from Zhoukoudian, Sangiran, West Turkana, East Rudolf, Olduvai and Dmanisi. Middle Pleistocene African archaics (MPAf) include individuals from Thomas Quarries, Salé, Rabat, Hoedijespunt, Cave of Hearths, Olduvai, Kaphthurin, Eyasi, Broken Hill and Sidi Abderrahmane. Middle Pleistocene European archaics (MPE) include individuals from Mauer, Arago, Sima de los Huesos, Fontana Ranuccio. Neanderthal samples include individuals from Amud, Arcy sur Cure, Chateaufort, Combe Grenal, Cova Negra, Ehringdorf, Feldhofer, Grotta Guattari, Grotta Taddeo, Hortus, Kalamakia, Krapina, Kebara, Kulna, La Quina, La Fate, La Ferrassie, Le Moustier, Marillac, Melpignano, Mongaudier, Monsempron, Monte Fenera, Malarnaud, Montmaurin, Obi-Rakhmat, Ochoz, Pech-de-l'Azé, Petit Puymoyen, Pontnewydd, Rozhok, Regourdou, Roc-de-Marsal, Saccopastore, Saint-Césaire, Spy, Subalyuk, Taubach, Tabun and Vindija. EMH samples include individuals from Die Kelders, Equus Cave, Klasies River Mouth, Sea Harvest, Mumba, Haua Fteah, Dar es-Soltan, Contrebandiers, El Harhoura, Qafzeh and Skhul.

Data availability. The data that support the findings of this study are available from the corresponding authors upon reasonable request.

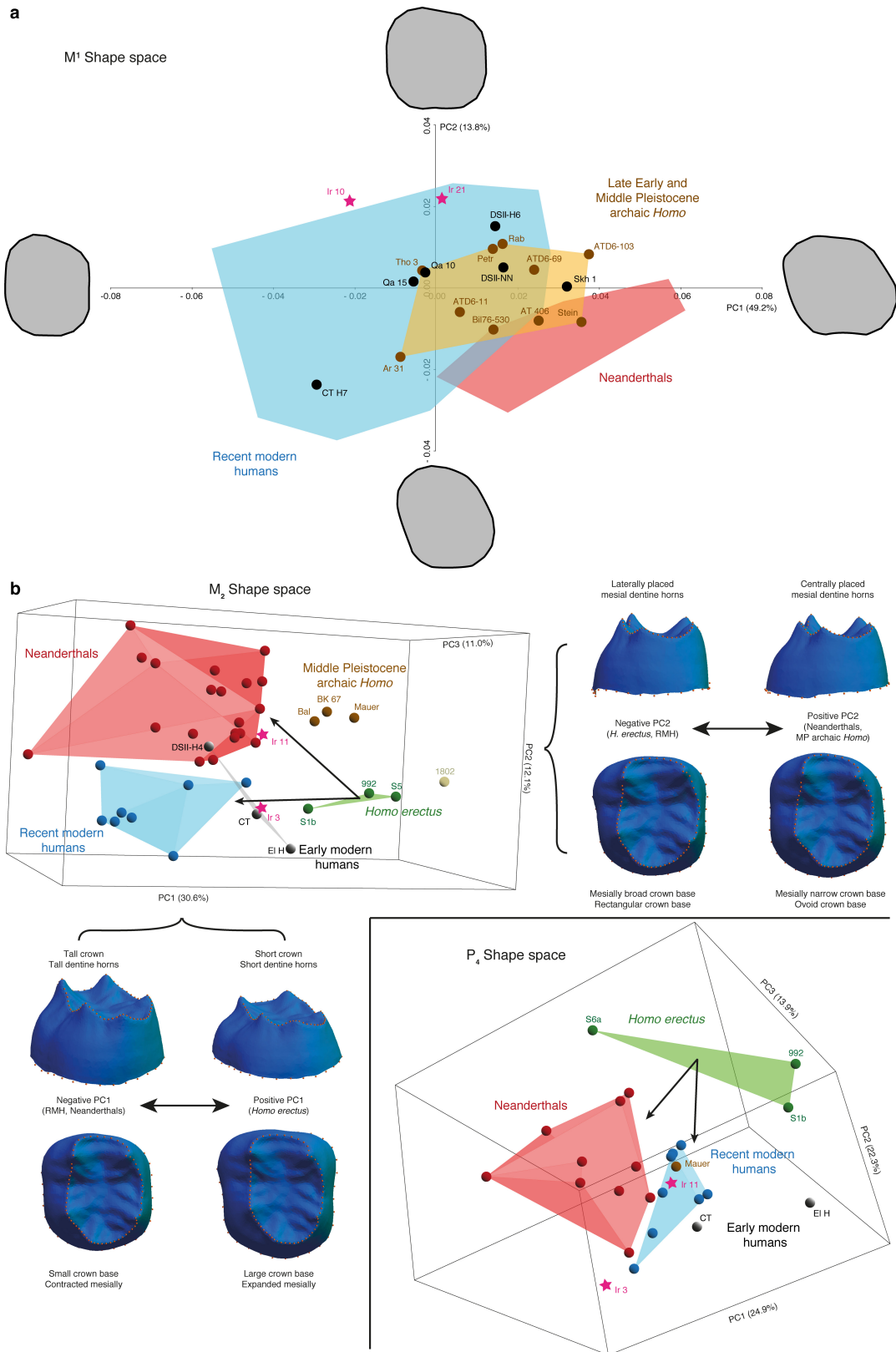
- Wollny, G. *et al.* MIA - a free and open source software for gray scale medical image analysis. *Source Code Biol. Med.* **8**, 20 (2013).
- Bookstein, F. L. Landmark methods for forms without landmarks: morphometrics of group differences in outline shape. *Med. Image Anal.* **1**, 225–243 (1997).
- Gunz, P., Mitteroecker, P. & Bookstein, F. L. in *Modern Morphometrics in Physical Anthropology*. (ed. Slice, D.E.) 73–98 (Kluwer Academic/Plenum Publishers, 2005).
- Gunz, P. & Mitteroecker, P. Semilandmarks: a method for quantifying curves and surfaces. *Hystrix* **24**, 103–109 (2013).
- Wiley, D. F. *et al.* Evolutionary Morphing. In *16th IEEE Visualization Conference (VIS 2005)* **55**, 431–438 (American Journal of Physical Anthropology, 2005).
- Freidline, S. E., Gunz, P., Harvati, K. & Hublin, J.-J. Middle Pleistocene human facial morphology in an evolutionary and developmental context. *J. Hum. Evol.* **63**, 723–740 (2012).
- Neubauer, S., Gunz, P. & Hublin, J.-J. The pattern of endocranial ontogenetic shape changes in humans. *J. Anat.* **215**, 240–255 (2009).
- Harvati, K., Gunz, P. & Grigorescu, D. Cioclovina (Romania): affinities of an early modern European. *J. Hum. Evol.* **53**, 732–746 (2007).
- Benazzi, S. *et al.* Early dispersal of modern humans in Europe and implications for Neanderthal behaviour. *Nature* **479**, 525–528 (2011).
- Bailey, S. E., Benazzi, S. & Hublin, J.-J. Allometry, merism, and tooth shape of the upper deciduous M2 and permanent M1. *Am. J. Phys. Anthropol.* **154**, 104–114 (2014).
- Benazzi, S. *et al.* Cervical and crown outline analysis of worn Neanderthal and modern human lower second deciduous molars. *Am. J. Phys. Anthropol.* **149**, 537–546 (2012).
- Skinner, M. M., Gunz, P., Wood, B. A. & Hublin, J.-J. Enamel–dentine junction (EDJ) morphology distinguishes the lower molars of *Australopithecus africanus* and *Paranthropus robustus*. *J. Hum. Evol.* **55**, 979–988 (2008).
- Skinner, M. M., Gunz, P., Wood, B. A., Boesch, C. & Hublin, J.-J. Discrimination of extant *Pan* species and subspecies using the enamel–dentine junction morphology of lower molars. *Am. J. Phys. Anthropol.* **140**, 234–243 (2009).
- Spoor, F. *et al.* Reconstructed *Homo habilis* type OH 7 suggests deep-rooted species diversity in early *Homo*. *Nature* **519**, 83–86 (2015).
- Beucher, S. & Lantuéjoul, C. in *International Workshop on Image Processing: Real-Time Edge and Motion Detection 2.1–2.12* (Rennes, France, 1979).
- Le Cabec, A., Gunz, P., Kupczik, K., Braga, J. & Hublin, J.-J. Anterior tooth root morphology and size in Neanderthals: taxonomic and functional implications. *J. Hum. Evol.* **64**, 169–193 (2013).
- Mitteroecker, P. & Gunz, P. Advances in geometric morphometrics. *Evol. Biol.* **36**, 235–247 (2009).

48. Gunz, P., Mitteroecker, P., Neubauer, S., Weber, G. W. & Bookstein, F. L. Principles for the virtual reconstruction of hominin crania. *J. Hum. Evol.* **57**, 48–62 (2009).
49. Rohlf, F. J. & Slice, D. Extensions of the procrustes method for the optimal superimposition of landmarks. *Syst. Zool.* **39**, 40–59 (1990).
50. Mitteroecker, P. & Bookstein, F. Linear discrimination, ordination, and the visualization of selection gradients in modern morphometrics. *Evol. Biol.* **38**, 100–114 (2011).
51. R Development Core Team. R: a language and environment for statistical computing <http://www.r-project.org> (R Foundation for Statistical Computing, Vienna, Austria, 2012).
52. Arambourg, C. & Biberson, P. The fossil human remains from the Paleolithic site of Sidi Abderrahman (Morocco). *Am. J. Phys. Anthropol.* **14**, 467–489 (1956).
53. Sausse, F. La mandibule atlanthropienne de la carrière Thomas I (Casablanca). *Anthropologie* **79**, 81–112 (1975).
54. Rightmire, G. P. Comparative studies of Late Pleistocene human remains from Klasies River Mouth, South Africa. *J. Hum. Evol.* **20**, 131–156 (1991).
55. Stewart, T. D. in *Annual Report of the Smithsonian Institution* 521–533 (US Government Printing Office, Washington, 1962).
56. Tillier, A.-M. in *Le Squelette moustérien de Kébara* 2 97–112 (Centre National de la Recherche Scientifique, Paris, 1991).
57. Stewart, T. D. The Neanderthal skeletal remains from Shanidar Cave, Iraq: a summary of findings to date. *Proc. Am. Phil. Soc.* **121**, 121–165 (1977).
58. Trinkaus, E. *The Shanidar Neanderthals* (Academic, 1983).
59. Leroi-Gourhan, A. *Étude des Restes Humains Fossiles provenant des Grottes d'Arcy-sur-Cure* (Masson et Cie, 1958).
60. Daura, J. et al. A Neandertal mandible from the Cova del Gegant (Sitges, Barcelona, Spain). *J. Hum. Evol.* **49**, 56–70 (2005).
61. Topinard, P. Les caractères simiens de la machoire de la Naulette. *Rev. Antropol.* **15**, 385–431 (1886).
62. Blake, C. C. On a human jaw from the cave of La Naulette, near Dinant, Belgium. *Anthropol. Rev.* **5**, 294–303 (1867).
63. Leguebe, A. & Toussaint, M. *La Mandibule et les Cubitus de la Naulette: Morphologie et Morphométrie* 15 (Editions du Centre National de la Recherche Scientifique, 1988).
64. Heim, J. L. Les hommes fossiles de La Ferrassie (Dordogne) et le problème de la définition des Neandertaliens classiques. III. Squelette céphalique. *Anthropologie* **78**, 321–378 (1974).
65. de Lumley, M.-A. Les Néandertaliens de la grotte de l'Hortus. *Études Quaternaires* **1**, 375–385 (1972).
66. Condemni, S. et al. Possible interbreeding in late Italian Neanderthals? New data from the Mezzena jaw (Monti Lessini, Verona, Italy). *PLoS ONE* **8**, e59781 (2013).
67. Corrain, C. Resti scheletrici umani del 'Riparo Mezzena'. *Memorie del Museo civico di Storia naturale di Verona* **16**, 97–101 (1968).
68. Walker, M. J., Lombardi, A. V., Zapata, J. & Trinkaus, E. Neandertal mandibles from the Sima de las Palomas del Cabezo Gordo, Murcia, southeastern Spain. *Am. J. Phys. Anthropol.* **142**, 261–272 (2010).
69. Martin, H. Machoire humaine moustérienne trouvée dans la station de La Quina. *L'homme préhistorique* **13**, 3–21 (1926).
70. Martin, H. Position stratigraphique des Ossements humains recueillis dans le Moustérien de La Quina de 1908 à 1912. *Bull. Soc. Préhistorique* **9**, 700–709 (1912).
71. Martin, H. *L'Homme fossile de la Quina*. (Librairie Octave Doin, 1923).
72. Pap, I., Tillier, A. M., Arensburg, B. & Chech, M. The Subalyuk Neanderthal remains (Hungary): a re-examination. *Ann. Hist. Nat. Mus. Natl. Hung.* **88**, 233–270 (1996).
73. Sanchez, F. Comparative biometrical study of the Mousterian mandible from Cueva del Boquete de Zafarraya (Málaga, Spain). *Hum. Evol.* **14**, 125–138 (1999).
74. Vlček, E. *Fossile Menschenfunde von Weimar-Ehringsdorf*, Weimarer Monographien zur Ur- und Frühgeschichte Vol. 30 (Landesamt für Archäologische Denkmalpflege, 1993).
75. Condemni, S. *Les néandertaliens de La Chaise: abri Bourgeois-Delaunay. Comité des travaux historiques et scientifiques* (CTHS, 2001).
76. Bar-Yosef, O. & Vandermeersch, B. (eds) *Le squelette moustérien de Kébara 2*. (Editions du Centre National de la Recherche Scientifique, 1991).
77. Arambourg, C. & Hoffstetter, R. *Le gisement de Ternifine* Vol. 1. (Masson, 1963).
78. Hooton, E.A., Hencken, H.O & Snow, Ch. E. *The ancient Palestinian: Skhul V reconstruction*. **17**, 5–10 (American School of Prehistoric Research, 1953).
79. Sollas, W. J. The Chancelade skull. *J. R. Anthropol. Inst.* **57**, 89–122 (1927).
80. Martin, H. Caractères des squelettes humains quaternaires de la vallée du Roc (Charente). *Bull. Mem. Soc. Anthropol. Paris* **8**, 103–129 (1927).
81. Vercellotti, G., Alciati, G., Richards, M. P. & Formicola, V. The Late Upper Paleolithic skeleton Villabruna 1 (Italy): a source of data on biology and behavior of a 14,000 year-old hunter. *J. Anthropol. Sci.* **86**, 143–163 (2008).
82. Formicola, V. Una mandibola umana dal deposito dell'Epigravettiano finale delle Arene Candide (scavi 1970). *Rev. Antropol.* **64**, 271–278 (1986).
83. Odano, A. M. & Riquet, R. Le gisement préhistorique de Dar-es-Soltane 2. Champ de tir de El Menzeh à Rabat (Maroc). Note préliminaire. 2. Étude anthropologique des restes post-atériens. *Bull. d'Archéologie Marocaine* **11**, 25–63 (1978).
84. Debénath, A. Nouveaux restes humains atériens du Maroc. *CR Acad. Sci. Paris* **290**, 851–852 (1980).
85. Crognier, E. & Dupouy-Madre, M. Les Natoufiens du Nahal Oren (Ouadi Fallah) Étude anthropologique. *Paéorient* **2**, 103–121 (1974).
86. Henke, W. Vergleichend-morphologische Kennzeichnung der Jungpaläolithiker von Oberkassel bei Bonn. *Z. Morphol. Anthropol.* **75**, 27–44 (1984).
87. Hershkovitz, I. et al. Ohalo II H2: a 19,000-year-old skeleton from a water-logged site at the Sea of Galilee, Israel. *Am. J. Phys. Anthropol.* **96**, 215–234 (1995).
88. Soficaru, A., Dobos, A. & Trinkaus, E. Early modern humans from the Pestera Muierii, Baia de Fier, Romania. *Proc. Natl Acad. Sci. USA* **103**, 17196–17201 (2006).
89. Crevecoeur, I. *Étude anthropologique des restes humains de Nazlet Khater (Paléolithique Supérieur, Égypte)*. PhD Thesis, Université Sciences et Technologies Bordeaux I (2006).
90. Thoma, A. Morphology and affinities of the Nazlet Khater man. *J. Hum. Evol.* **13**, 287–296 (1984).
91. Anderson, J. E. In *The Prehistory of Nubia* Vol. 2 (ed. Wendorf, F.) 996–1040 (Southern Methodist Univ. Press, 1968).
92. Crevecoeur, I. From the Nile to the Danube: a comparison of the Nazlet Khater 2 and Oase 1 early modern human mandibles. *Anthropologie* **42**, 203–213 (2004).
93. Trinkaus, E. et al. An early modern human from the Peștera cu Oase, Romania. *Proc. Natl Acad. Sci. USA* **100**, 11231–11236 (2003).
94. Trinkaus, E. & Svoboda, J. (eds) *Early Modern Human Evolution in Central Europe. The People of Dolní Věstonice and Pavlov*. The Dolni Vestonice Studies Vol. 12 (Oxford Univ. Press, 2006).
95. Sládek, V., Trinkaus, E., Hillson, S. W. & Holliday, T. W. *The People of the Pavlovian. Skeletal Catalogue and Osteometrics of the Gravettian Fossil Hominids from Dolni Vestonice and Pavlov*. The Dolni Vestonice Studies Vol. 5 1–244 (BRNO, 2000).
96. Drozdová, E. The evaluation of a rediscovered fragment of human lower jaw, No 21 from Předmostí u Přerova. *Archeologické rozhledy* **53**, 452–460 (2001).
97. Dutour, O. Palimpseste paléolithique sur l'«Homme fossile d'Asselar» (Sahara). *Travaux du Laboratoire d'Anthropologie et de Préhistoire des Pays de la Méditerranée Occidentale* **1**, 73–83 (1992).
98. Gambier, D. Vestiges humains du gisement d'Isturitz (Pyrénées—Atlantiques): étude anthropologique et analyse des traces d'action humaine intentionnelle. *Antiquités nationales* **22–23**, 9–26 (1990).
99. Bräuer, G. & Mehlman, M. J. Hominid molars from a middle Stone Age level at the Mumba Rock Shelter, Tanzania. *Am. J. Phys. Anthropol.* **75**, 69–76 (1988).
100. Protsch, R. R. R. *Di Archäologischen und Anthropologischen Ergebnisse der Kohl-Larsen-Expeditionen in Nord-Tanzania 1933–1939*. (Institut für Urgeschichte der Universität Tübingen, 1981).
101. Wood, B. A. & Van Noten, F. L. Preliminary observations on the BK 8518 mandible from Baringo, Kenya. *Am. J. Phys. Anthropol.* **69**, 117–127 (1986).
102. Rightmire, G. P. Middle Pleistocene hominids from Olduvai Gorge, northern Tanzania. *Am. J. Phys. Anthropol.* **53**, 225–241 (1980).
103. Bermúdez de Castro, J. M. Dental remains from Atapuerca (Spain) I. Metrics. *J. Hum. Evol.* **15**, 265–287 (1986).
104. Grine, F. E. & Franzen, J. L. Fossil hominid teeth from the Sangiran Dome (Java, Indonesia). *Courier Forschungsinstitut Senckenberg* **171**, 75–103 (1994).
105. Le Cabec, A., Gunz, P., Kupczik, K., Braga, J. & Hublin, J.-J. Anterior tooth root morphology and size in Neanderthals: taxonomic and functional implications. *J. Hum. Evol.* **64**, 169–193 (2013).
106. Turner, C. G. II, Nichol, C. R. & Scott, G. R. *Advances in Dental Anthropology* (eds Kelley, M., & Larsen, C.) 13–31 (Wiley Liss, 1991).
107. Bailey, S. E. *Neandertal Dental Morphology: Implications for modern human origins*. PhD thesis, Arizona State Univ. (2002).



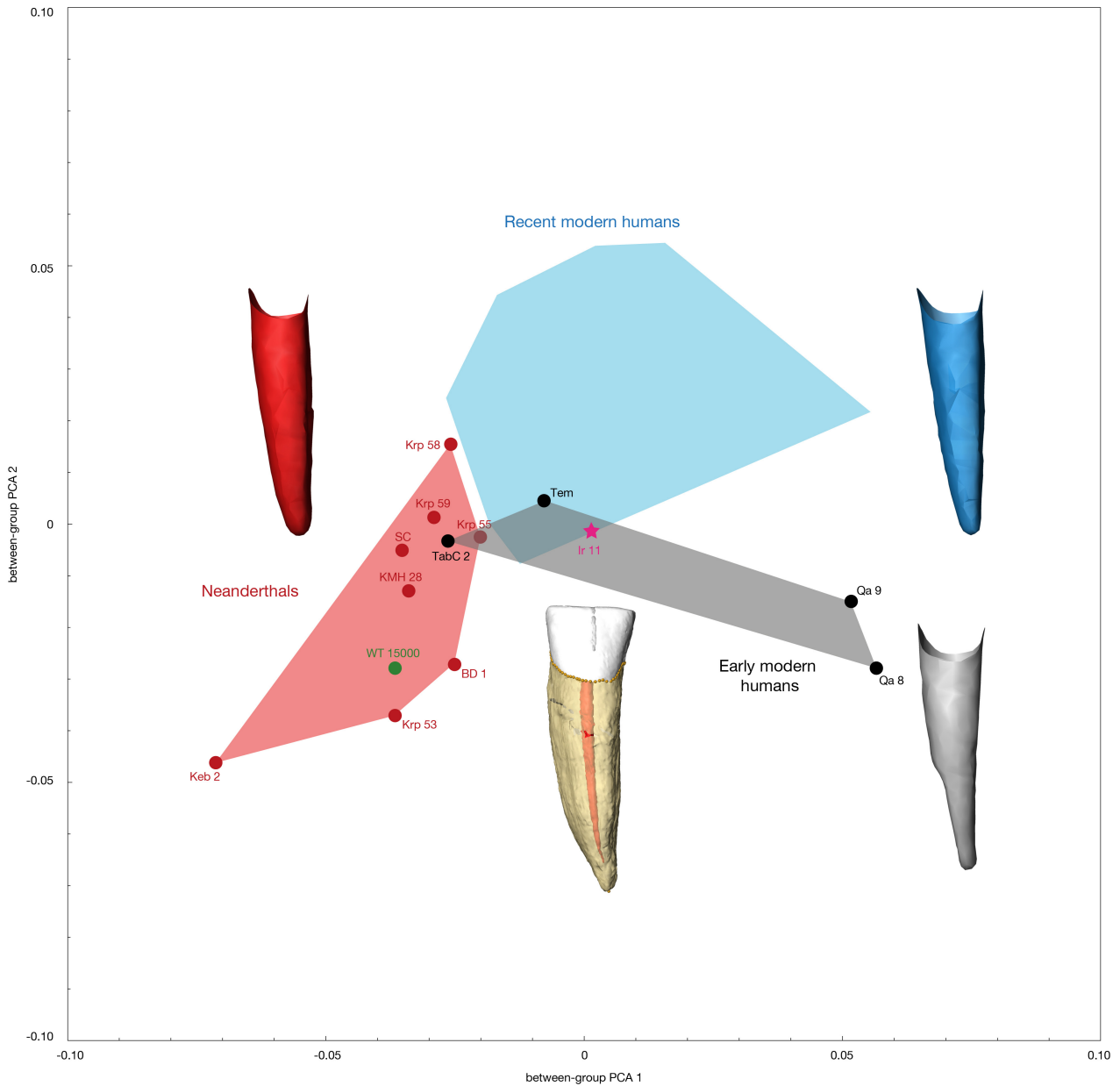
Extended Data Figure 1 | Mandibular morphology. a, Symphyseal section of the Irhoud 11 mandible showing the mental angle. b, Mental area of Irhoud 11 before virtual reconstruction (top) and Irhoud 3 (bottom). Both images are surface models generated from micro-computed tomography data. c, Bivariate plot of mandibular corpus breadth

versus height at the mental foramen. Irhoud 11 (pink star) falls within the EMH distribution and has one of the largest corpus heights among Middle to Late Pleistocene hominins. Values are in mm. *n* indicates sample size. Data sources and sample compositions can be found in the Methods. Scale bar, 20 mm.



Extended Data Figure 2 | Dental morphology. a, Shape-space PCA plot of Late Early and Middle Pleistocene archaic *Homo*, Neanderthals and RMH M₁ crown outlines. The deformed mean crown outlines in the four directions of the PCs are drawn at the extremity of each axis. Sample compositions and abbreviations can be found in the Methods. **b**, EDJ morphology of the M₂ and P₄. Top left, the PCA analysis of the EDJ shape of the M₂ places Irhoud 11 intermediate between *H. erectus*

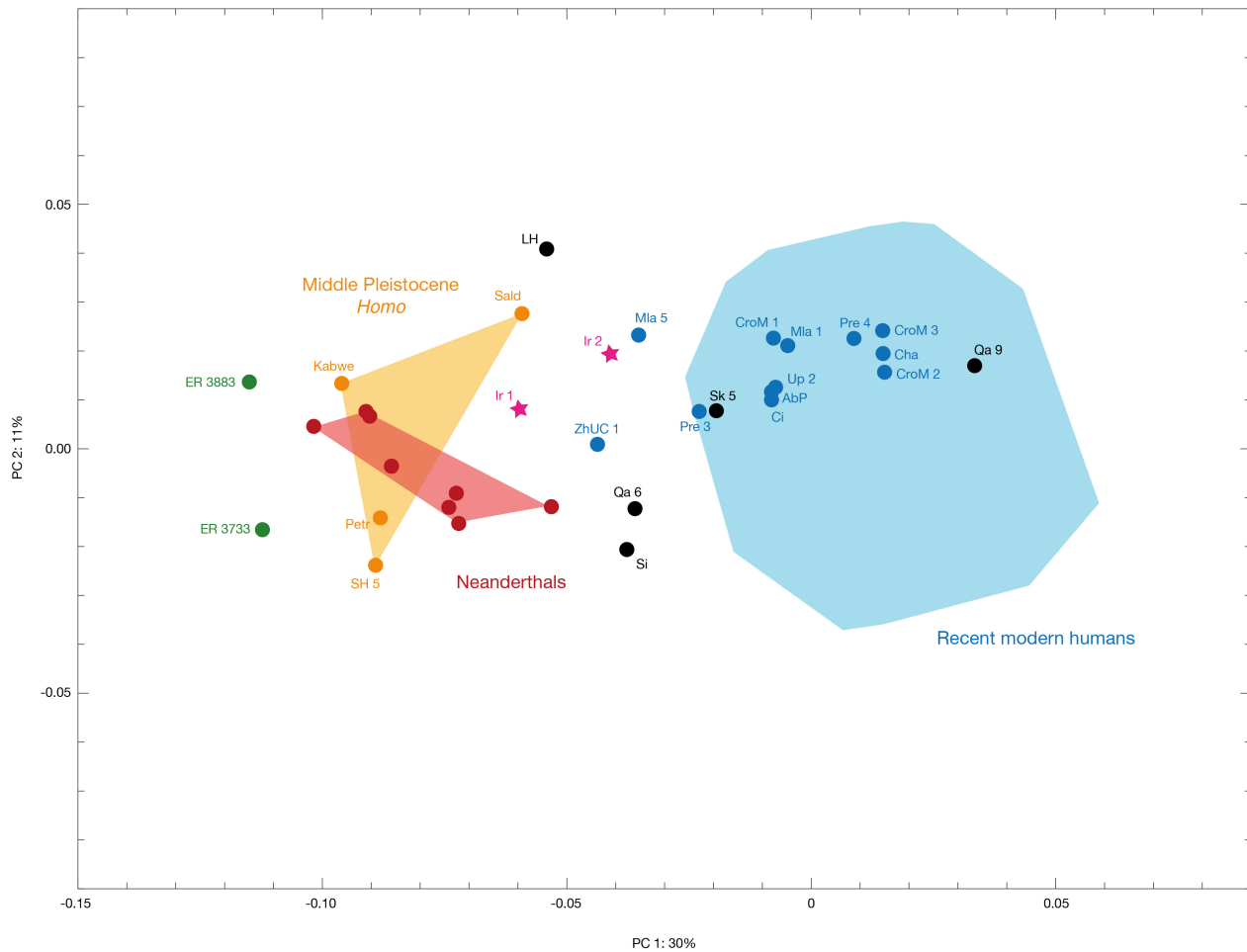
and RMH (along with other north Africa fossil humans) and distinct from Neanderthals. Surface models illustrate EDJ shape changes along PC1 (bottom left) and PC2 (top right); the former separating *H. erectus* from RMH, Neanderthals and north African EMH and the latter separating Neanderthals from RMH and north African EMH. Bottom right, a PCA analysis of the EDJ shape of the P₄ groups Irhoud 11 with modern and fossil humans.



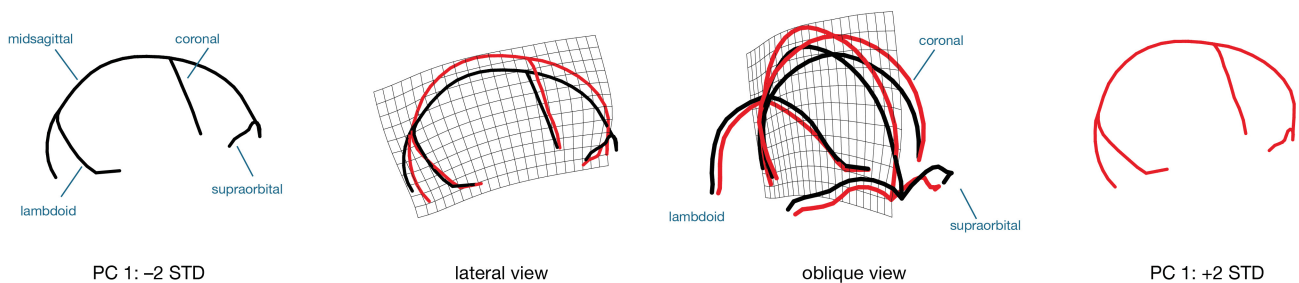
Extended Data Figure 3 | Shape analysis of I_2 roots. A between-group PCA shows a complete separation between Neanderthals and a worldwide sample of recent modern humans based on subtle shape differences. Irhoud 11 (pink star) plots at the fringes of RMH, close to the EMH from Contrebandiers 1 (Tem). Colour-coded Procrustes group mean shapes are plotted in the same orientation as the I_2 root surface of Irhoud 11. Although Irhoud 11 is more similar, overall, to Neanderthals in terms

of root size, its root shape is clearly modern. The *H. erectus* specimen KNM-WT 15000 and hypothetical EMH Tabun C2 have incisor root shapes similar to Neanderthals, suggesting that roots that are labially more convex than in RMH represent a conserved primitive condition with limited taxonomical value. Sample compositions and abbreviations can be found in the Methods.

a Principal component analysis: Shape of the external vault



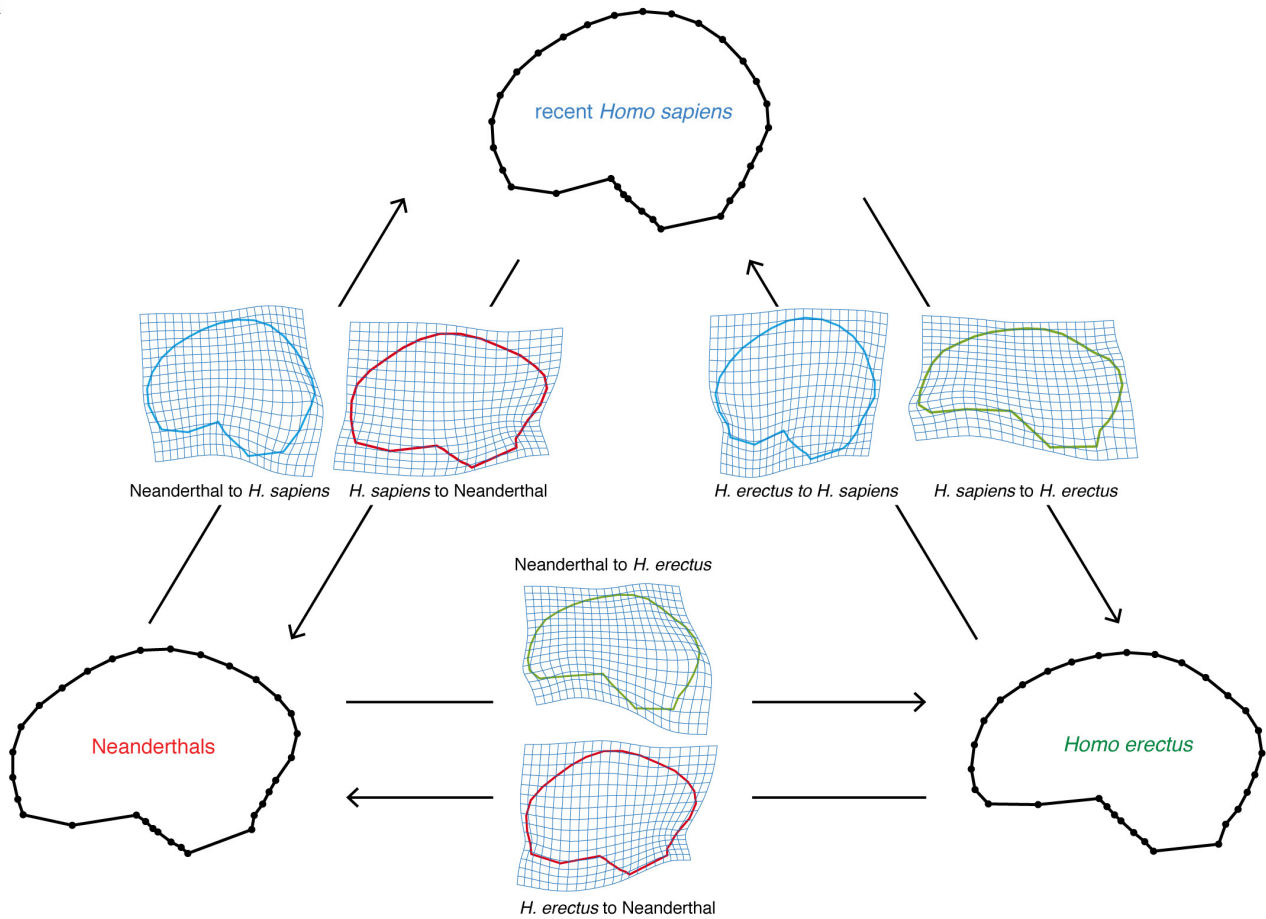
b



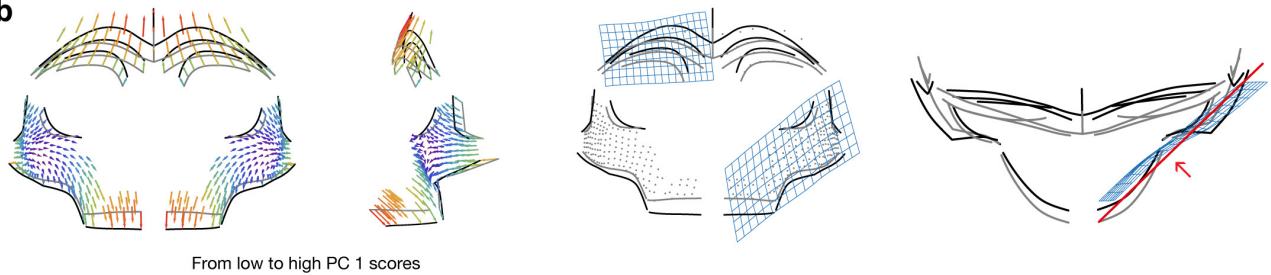
Extended Data Figure 4 | Shape analysis of the external vault. **a**, PC scores of PC1 and PC2 of external braincase shape in *H. erectus*, archaic Middle Pleistocene *Homo*, geographically diverse RMH and Neanderthals. Results are consistent with the analysis of endocranial shape (Fig. 3a). However, several EMH and Upper Palaeolithic specimens fall outside the RMH variation. This is probably owing to the projecting supraorbital tori in these specimens. **b**, Shape changes associated with PC1 (two standard

deviations in either direction) shown as thin-plate spline deformation grids in lateral and oblique view. PC1 captures a contrast between elongated braincases with projecting supraorbital tori (low scores, in black) and a more globular braincase with gracile supraorbital tori (high scores, in red). Sample compositions and abbreviations can be found in the Methods.

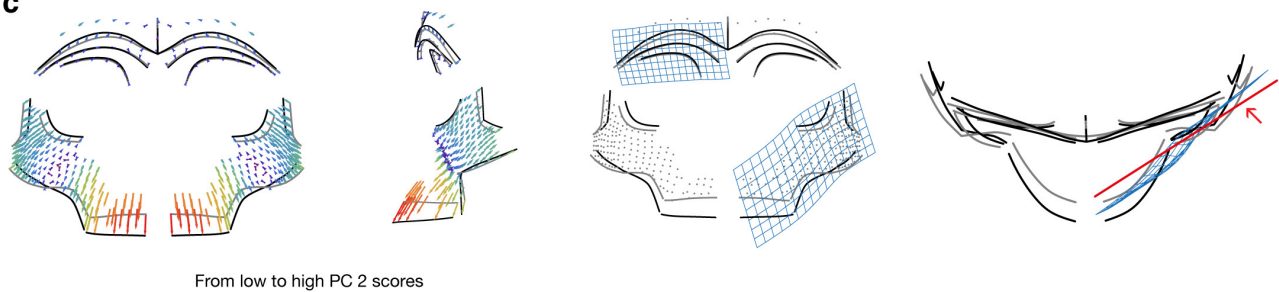
a



b



c



Extended Data Figure 5 | Facial and endocranial shape differences among *Homo* groups. Visualizations of GMM shape analyses in Fig. 3. **a**, Average endocranial shape differences between *H. erectus*, recent *H. sapiens* and Neanderthals. Thin-plate spline grids are exaggerated. **b**, Visualization of shape changes along PC1 in Fig. 3b in frontal, lateral and superior view; two standard deviations in either direction from the mean shape (grey, negative; black, positive). **c**, Shape changes along PC2.

All recent and fossil modern humans (low scores along PC2) share smaller, orthognathic faces, that differ from the larger, robust and prognathic faces of the Middle Pleistocene humans and Neanderthals (high scores along PC1). Arrow length is colour-coded (short, blue; long, red). As these visualizations are affected by the Procrustes superimposition, we also show grids for the maxilla and the supraorbital area. The arrow points to the plane of the maxillary thin-plate spline (red) in the template configuration.

Extended Data Table 1 | List of hominin specimens

| Specimens | Item ID | Anatomical part | Year | Stratigraphic position |
|-----------|------------------------------|-------------------------------------|---------|--|
| Irhoud 1 | No ID | Cranium | 1961 | Lower deposits ⁴ |
| Irhoud 2 | No ID | Cranium | 1962 | Lower deposits ⁴ |
| Irhoud 3 | No ID | Mandible (juvenile) | 1968 | Lower deposits ⁵ |
| Irhoud 4 | No ID | Humerus (juvenile) | 1969 | Layer 18 of Tixier ⁶ |
| Irhoud 5 | No ID | Coxal (juvenile) | 1969 | Layer 18 of de Bayle des Hermens & Tixier ⁷ |
| Irhoud 6 | No ID | Mandible fragment | 1961-69 | Identified among faunal remains |
| Irhoud 7 | 4766 | Lower right first premolar | 2004 | Initial cleaning |
| Irhoud 8 | 4767 | Distal part of left lower molar | 2004 | Initial cleaning |
| Irhoud 9 | 1653 | First or second lower molar | 2006 | Layer 4 |
| Irhoud 10 | 1678, 1679, 1680, 2178, 2259 | Cranium | 2007 | Layer 7 |
| Irhoud 11 | 4765 + 3752 | Mandible | 2007 | Layer 7 |
| Irhoud 12 | 2196 | Lower incisor | 2007 | Layer 7 |
| Irhoud 13 | 2252 | Left proximal femur | 2007 | Layer 7 |
| Irhoud 14 | 2381, 2383 | Rib | 2009 | Layer 7 |
| Irhoud 15 | 2401 | Rib | 2009 | Layer 7 |
| Irhoud 16 | 2561, 2565 | Humerus (juvenile) | 2009 | Layer 7 |
| Irhoud 17 | 2670 | Right proximal femur | 2009 | Layer 7 |
| Irhoud 18 | 2838 | Lumbar vertebra | 2007 | Initial cleaning |
| Irhoud 19 | 3747, 3748, 3749 | Fibula | 2009 | Layer 7 |
| Irhoud 20 | 3751 | Cervical vertebra | 2009 | Initial cleaning |
| Irhoud 21 | 4200 | Maxilla | 2011 | Layer A |
| Irhoud 22 | 4502, 4503 | Upper second and third right molars | 2011 | Layer A |

Starting with the 2004 excavation, specimens were given identification numbers from the project catalogue. Layer 18 of the excavation in ref. 6 corresponds to Layer 7 of the 2004–2011 excavation. MPAf, archaic Middle Pleistocene African specimens; MPE, archaic Middle Pleistocene European specimens.

Extended Data Table 2 | Measurements of the Irhoud 11 mandible after reconstruction

| Measurement | Irhoud 11 | African and European archaic MP | Asian Neanderthals | European Neanderthals | Early modern humans | Upper Palaeolithic MH |
|--|-----------|--|--|--|--|--|
| <i>Symphyseal Height</i> | 45 | $\bar{x} = 31.53$ $\sigma = 3.7$ $n = 13$ | $\bar{x} = 36.1$ $\sigma = 3.36$ $n = 6$ | $\bar{x} = 33.98$ $\sigma = 4.64$ $n = 21$ | $\bar{x} = 36.36$ $\sigma = 6.03$ $n = 8$ | $\bar{x} = 31.87$ $\sigma = 2.82$ $n = 38$ |
| <i>Corpus Height at Mental Foramen</i> | 38.4 | $\bar{x} = 30.69$ $\sigma = 4.2$ $n = 19$ | $\bar{x} = 33.9$ $\sigma = 3.51$ $n = 7$ | $\bar{x} = 31.22$ $\sigma = 3.43$ $n = 33$ | $\bar{x} = 34.23$ $\sigma = 4.57$ $n = 13$ | $\bar{x} = 30.89$ $\sigma = 3.11$ $n = 47$ |
| <i>Corpus Breadth at Mental Foramen</i> | 15.4 | $\bar{x} = 17.22$ $\sigma = 1.98$ $n = 19$ | $\bar{x} = 17.16$ $\sigma = 1.89$ $n = 7$ | $\bar{x} = 15.56$ $\sigma = 1.71$ $n = 33$ | $\bar{x} = 16.04$ $\sigma = 1.75$ $n = 13$ | $\bar{x} = 12.67$ $\sigma = 1.55$ $n = 48$ |
| <i>Corpus Height at M₁</i> | 36 | $\bar{x} = 31.15$ $\sigma = 4.59$ $n = 15$ | $\bar{x} = 31.65$ $\sigma = 3.17$ $n = 4$ | $\bar{x} = 30.82$ $\sigma = 3.36$ $n = 22$ | $\bar{x} = 32.81$ $\sigma = 5.64$ $n = 10$ | $\bar{x} = 29.51$ $\sigma = 2.19$ $n = 29$ |
| <i>Corpus Breadth at M₁</i> | 17.7 | $\bar{x} = 17.57$ $\sigma = 2.4$ $n = 15$ | $\bar{x} = 17.54$ $\sigma = 2.67$ $n = 5$ | $\bar{x} = 16.7$ $\sigma = 1.75$ $n = 22$ | $\bar{x} = 17.11$ $\sigma = 2.57$ $n = 11$ | $\bar{x} = 14.25$ $\sigma = 1.57$ $n = 26$ |
| <i>Corpus Height at M₁/M₂</i> | 34 | $\bar{x} = 30.82$ $\sigma = 4.21$ $n = 15$ | $\bar{x} = 32.40$ $\sigma = 1.65$ $n = 3$ | $\bar{x} = 29.64$ $\sigma = 3.21$ $n = 23$ | $\bar{x} = 32.88$ $\sigma = 4.26$ $n = 8$ | $\bar{x} = 28.64$ $\sigma = 2.3$ $n = 33$ |
| <i>Corpus Breadth at M₁/M₂</i> | 19.3 | $\bar{x} = 18.03$ $\sigma = 2.98$ $n = 15$ | $\bar{x} = 17.57$ $\sigma = 2.25$ $n = 3$ | $\bar{x} = 16.35$ $\sigma = 1.56$ $n = 22$ | $\bar{x} = 17.56$ $\sigma = 2.43$ $n = 8$ | $\bar{x} = 14.73$ $\sigma = 1.92$ $n = 34$ |
| <i>Corpus Height at M₂</i> | 31,5 | $\bar{x} = 30.42$ $\sigma = 3.97$ $n = 20$ | $\bar{x} = 31.75$ $\sigma = 3.82$ $n = 6$ | $\bar{x} = 30.10$ $\sigma = 3.4$ $n = 26$ | $\bar{x} = 32.41$ $\sigma = 5.22$ $n = 8$ | $\bar{x} = 27.04$ $\sigma = 2.58$ $n = 34$ |
| <i>Corpus Breadth at M₂</i> | 22.7 | $\bar{x} = 18.45$ $\sigma = 2.45$ $n = 20$ | $\bar{x} = 17.6$ $\sigma = 1.54$ $n = 7$ | $\bar{x} = 16.03$ $\sigma = 1.78$ $n = 25$ | $\bar{x} = 18.48$ $\sigma = 2.93$ $n = 8$ | $\bar{x} = 15.02$ $\sigma = 1.89$ $n = 36$ |
| <i>Length of the Dental Arcade</i> | 66.5 | $\bar{x} = 58.19$ $\sigma = 5.46$ $n = 11$ | $\bar{x} = 54.78$ $\sigma = 2.78$ $n = 4$ | $\bar{x} = 55.23$ $\sigma = 2.49$ $n = 10$ | $\bar{x} = 57.25$ $\sigma = 6.22$ $n = 4$ | $\bar{x} = 51.78$ $\sigma = 3.33$ $n = 26$ |
| <i>Bigonial Breadth</i> | 144 ? | $\bar{x} = 96.93$ $\sigma = 11.84$ $n = 6$ | $\bar{x} = 102.13$ $\sigma = 6.22$ $n = 4$ | $\bar{x} = 92.57$ $\sigma = 11.62$ $n = 6$ | $\bar{x} = 93.75$ $\sigma = 13.93$ $n = 4$ | $\bar{x} = 98.59$ $\sigma = 9.67$ $n = 29$ |
| <i>Bicanine Breadth</i> | 38.5 | $\bar{x} = 35.54$ $\sigma = 3.79$ $n = 11$ | $\bar{x} = 36.48$ $\sigma = 1.63$ $n = 6$ | $\bar{x} = 36.62$ $\sigma = 2.45$ $n = 14$ | $\bar{x} = 38.0$ $\sigma = 2.00$ $n = 5$ | $\bar{x} = 32.64$ $\sigma = 2.38$ $n = 28$ |
| <i>Bi-M₂ Breadth</i> | 66.6 | $\bar{x} = 66.13$ $\sigma = 5.81$ $n = 11$ | $\bar{x} = 72.1$ $\sigma = 1.48$ $n = 4$ | $\bar{x} = 69.86$ $\sigma = 3.23$ $n = 11$ | $\bar{x} = 68.46$ $\sigma = 3.54$ $n = 5$ | $\bar{x} = 61.75$ $\sigma = 3.88$ $n = 26$ |
| <i>Bi-M₃ Breadth</i> | 70.9 | $\bar{x} = 70.24$ $\sigma = 6.22$ $n = 11$ | $\bar{x} = 74.86$ $\sigma = 2.78$ $n = 5$ | $\bar{x} = 71.9$ $\sigma = 3.29$ $n = 11$ | $\bar{x} = 72.03$ $\sigma = 4.16$ $n = 4$ | $\bar{x} = 66.62$ $\sigma = 4.07$ $n = 26$ |

The mandibles are compared to those of five groups of fossil hominins. Values are in mm. \bar{x} is the mean, σ is the standard deviation, n indicates sample size. The value with a ? is an estimate. Bi-M, Bimolar. Data sources and sample compositions can be found in the Methods

Extended Data Table 3 | Dental measurements (upper dentition)

| | | Irhoud 10 | Irhoud 21 | Irhoud 22 | <i>H. erectus</i> | MPE | MPAf | Neanderthals | EMH | RMH |
|----------------|----|-----------|-----------|-----------|--|--|---|--|--|--|
| C ¹ | BL | -- | 9.8 | -- | $\bar{x} = 10.3$ [9.7-11.9] $\sigma = 0.7$ n=12 | $\bar{x} = 9.8$ [8.8-10.7] $\sigma = 0.7$ n=6 | $\bar{x} = 9.7$ [8.9-10.5] $\sigma = 1.1$ n=2 | $\bar{x} = 10.0$ [8.8-11.4] $\sigma = 0.7$ n=26 | $\bar{x} = 9.3$ [8.5-10.4] $\sigma = 0.6$ n=11 | $\bar{x} = 8.3$ [7.0-9.8] $\sigma = 0.7$ n=131 |
| | MD | -- | 8.9 | -- | $\bar{x} = 9.6$ [8.5-10.3] $\sigma = 0.6$ n=11 | $\bar{x} = 8.7$ [7.7-9.9] $\sigma = 0.8$ n=7 | $\bar{x} = 9.3$ [8.9-9.6] $\sigma = 0.5$ n=2 | $\bar{x} = 8.8$ [7.0-10.0] $\sigma = 0.6$ n=24 | $\bar{x} = 8.4$ [7.5-9.7] $\sigma = 0.6$ n=10 | $\bar{x} = 7.7$ [6.2-8.8] $\sigma = 0.5$ n=122 |
| P ³ | BL | -- | 11.6 | -- | $\bar{x} = 11.7$ [10.4-12.9] $\sigma = 0.9$ n=12 | $\bar{x} = 10.9$ [10.5-12.1] $\sigma = 1.5$ n=7 | -- | $\bar{x} = 10.7$ [9.1-11.9] $\sigma = 0.8$ n=30 | $\bar{x} = 10.4$ [10.0-11.1] $\sigma = 0.4$ n=10 | $\bar{x} = 9.4$ [7.9-11.2] $\sigma = 0.7$ n=197 |
| | MD | -- | 8.4 | -- | $\bar{x} = 8.3$ [7.4-9.1] $\sigma = 0.5$ n=14 | $\bar{x} = 8.8$ [8.0-10.7] $\sigma = 0.9$ n=7 | -- | $\bar{x} = 8.0$ [6.2-9.3] $\sigma = 0.7$ n=29 | $\bar{x} = 7.7$ [7.0-8.7] $\sigma = 0.6$ n=10 | $\bar{x} = 7.1$ [5.6-8.6] $\sigma = 0.6$ n=186 |
| P ⁴ | BL | -- | 11.3 | -- | $\bar{x} = 11.3$ [9.9-13.4] $\sigma = 0.9$ n=22 | $\bar{x} = 11.1$ [9.9-12.2] $\sigma = 0.6$ n=8 | $\bar{x} = 11.3$ - n=1 | $\bar{x} = 10.5$ [8.2-11.7] $\sigma = 0.7$ n=26 | $\bar{x} = 10.4$ [9.7-11.5] $\sigma = 0.6$ n=11 | $\bar{x} = 9.5$ [7.6-12.3] $\sigma = 0.8$ n=194 |
| | MD | -- | 8.3 | -- | $\bar{x} = 8.1$ [7.2-9.2] $\sigma = 0.6$ n=21 | $\bar{x} = 8.0$ [7.3-8.4] $\sigma = 0.4$ n=7 | $\bar{x} = 7.9$ - n=1 | $\bar{x} = 7.6$ [5.7-8.8] $\sigma = 0.9$ n=26 | $\bar{x} = 7.1$ [7.0-9.3] $\sigma = 0.8$ n=12 | $\bar{x} = 6.9$ [5.4-11.3] $\sigma = 0.8$ n=173 |
| M ¹ | BL | 12.7 | 12.7 | -- | $\bar{x} = 13.0$ [11.7-14.7] $\sigma = 0.9$ n=18 | $\bar{x} = 12.1$ [10.9-14.4] $\sigma = 1.1$ n=10 | $\bar{x} = 12.8$ [11.8-13.8] $\sigma = 1.0$ n=3 | $\bar{x} = 12.1$ [10.9-14.2] $\sigma = 0.8$ n=26 | $\bar{x} = 12.6$ [11.2-15.2] $\sigma = 1.3$ n=22 | $\bar{x} = 11.5$ [9.8-13.6] $\sigma = 0.7$ n=313 |
| | MD | (12.1) | 12.2 | -- | $\bar{x} = 11.8$ [10.0-13.6] $\sigma = 0.9$ n=21 | $\bar{x} = 11.5$ [10.5-12.7] $\sigma = 0.8$ n=10 | $\bar{x} = 12.4$ [10.0-12.4] $\sigma = 1.2$ n=3 | $\bar{x} = 11.4$ [8.5-13.6] $\sigma = 1.0$ n=24 | $\bar{x} = 11.5$ [9.9-13.9] $\sigma = 1.1$ n=21 | $\bar{x} = 10.7$ [8.7-13.3] $\sigma = 0.7$ n=279 |
| M ² | BL | 12.3 | 12.4 | 13.8 | $\bar{x} = 13.3$ [11.3-15.5] $\sigma = 1.2$ n=12 | $\bar{x} = 13.3$ [11.3-16.3] $\sigma = 1.3$ n=10 | $\bar{x} = 12.5$ [11.2-12.2] $\sigma = 0.5$ n=4 | $\bar{x} = 12.8$ [11.2-16.2] $\sigma = 1.0$ n=27 | $\bar{x} = 12.3$ [10.5-13.7] $\sigma = 1.0$ n=12 | $\bar{x} = 11.6$ [9.1-14.1] $\sigma = 1.0$ n=229 |
| | MD | 10.9 | 11.8 | 12.6 | $\bar{x} = 11.6$ [10.2-13.6] $\sigma = 1.2$ n=10 | $\bar{x} = 10.9$ [9.7-12.4] $\sigma = 0.9$ n=9 | $\bar{x} = 11.1$ [10.2-11.7] $\sigma = 0.8$ n=3 | $\bar{x} = 11.0$ [9.3-13.1] $\sigma = 1.1$ n=19 | $\bar{x} = 10.3$ [8.6-11.8] $\sigma = 0.8$ n=9 | $\bar{x} = 9.9$ [7.1-12.2] $\sigma = 0.9$ n=199 |
| M ³ | BL | -- | 12.4 | 13.3 | $\bar{x} = 12.2$ [10.4-15.3] $\sigma = 1.4$ n=11 | $\bar{x} = 11.9$ [10.1-13.3] $\sigma = 1.0$ n=7 | $\bar{x} = 11.0$ - n=1 | $\bar{x} = 12.2$ [8.6-14.2] $\sigma = 1.2$ n=21 | $\bar{x} = 11.7$ [9.7-13.5] $\sigma = 1.0$ n=8 | $\bar{x} = 11.1$ [7.6-14.4] $\sigma = 1.2$ n=129 |
| | MD | -- | 8.4 | 11.6 | $\bar{x} = 10.0$ [8.7-12.4] $\sigma = 1.0$ n=11 | $\bar{x} = 9.0$ [8.0-11.0] $\sigma = 0.9$ n=7 | $\bar{x} = 9.8$ - n=1 | $\bar{x} = 10.3$ [8.4-13.9] $\sigma = 1.1$ n=21 | $\bar{x} = 9.3$ [8.6-10.9] $\sigma = 0.5$ n=6 | $\bar{x} = 8.9$ [6.1-12.8] $\sigma = 1.1$ n=115 |

Teeth are identified by letters: C, canine; M, molar; P, premolar; BL, bucco-lingual width; MD, mesiodistal length. Values are in mm. \bar{x} is the mean; minimum and maximum values are between square brackets; σ is the standard deviation; n indicates sample size. Values in parentheses represent uncorrected measurements on worn or cracked teeth. Data sources and sample compositions are in the Methods.

Extended Data Table 4 | Dental measurements (lower dentition)

| | | Irhoud 3 | Irhoud 11 | <i>H. erectus</i> | MPE | MPAf | Neanderthals | EMH | RMH |
|----------------|----|----------|-----------|--|--|---|--|--|--|
| I ₁ | BL | -- | 6.9 | \bar{x} = 6.7 [6.4-6.9] σ = 0.4 n = 3 | \bar{x} = 6.9 [6.4-7.5] σ = 0.4 n = 6 | \bar{x} = 7.3 [7.2-7.4] σ = 0.2 n = 2 | \bar{x} = 7.4 [6.8-8.2] σ = 0.4 n = 15 | \bar{x} = 6.6 [5.8-7.6] σ = 0.6 n = 10 | \bar{x} = 5.8 [4.8-6.8] σ = 0.4 n = 137 |
| | MD | -- | (5.8) | \bar{x} = 6.1 [5.8-6.6] σ = 0.4 n = 3 | \bar{x} = 5.7 [4.9-7.5] σ = 0.5 n = 6 | \bar{x} = 6.2 [5.9-6.4] σ = 0.4 n = 2 | \bar{x} = 5.5 [4.3-6.3] σ = 0.5 n = 13 | \bar{x} = 5.6 [4.5-6.8] σ = 0.9 n = 10 | \bar{x} = 5.4 [4.2-6.8] σ = 0.4 n = 134 |
| | RL | -- | 16.1 | \bar{x} = 19.4 - n = 1 | \bar{x} = 16.5 - n = 1 | -- | \bar{x} = 17.2 [13.8-20.9] σ = 1.9 n = 17 | \bar{x} = 14.4 [13.7-16.6] σ = 1.2 n = 5 | \bar{x} = 12.7 [10.1-16.7] σ = 1.5 n = 39 |
| I ₂ | BL | -- | 7.6 | \bar{x} = 7.2 [6.8-8.3] σ = 0.7 n = 4 | \bar{x} = 7.5 [6.7-8.6] σ = 0.6 n = 10 | \bar{x} = 7.8 - n = 1 | \bar{x} = 7.7 [6.8-8.1] σ = 0.3 n = 17 | \bar{x} = 7.1 [6.4-8.0] σ = 0.6 n = 10 | \bar{x} = 6.2 [4.9-7.7] σ = 0.5 n = 146 |
| | MD | -- | (7.8) | \bar{x} = 7.4 [7.2-7.9] σ = 0.3 n = 3 | \bar{x} = 6.6 [6.3-7.8] σ = 0.4 n = 10 | \bar{x} = 7.4 - n = 1 | \bar{x} = 6.5 [5.2-7.5] σ = 0.5 n = 16 | \bar{x} = 6.6 [5.7-7.8] σ = 0.7 n = 9 | \bar{x} = 6.0 [5.0-6.8] σ = 0.5 n = 143 |
| | RL | -- | 18.0 | \bar{x} = 18.6 [17.1-20.1] n = 2 | \bar{x} = 16.7 - n = 1 | -- | \bar{x} = 18.4 [14.8-21.6] σ = 2.0 n = 15 | \bar{x} = 15.4 [13.7-17.3] σ = 1.6 n = 6 | \bar{x} = 14.1 [10.7-18.4] σ = 1.4 n = 47 |
| C ₁ | BL | 9.1 | 9.4 | \bar{x} = 8.8 [8.3-9.6] σ = 0.5 n = 5 | \bar{x} = 8.5 [5.9-9.8] σ = 1.1 n = 11 | \bar{x} = 8.8 [7.7-10.0] σ = 1.6 n = 2 | \bar{x} = 9.2 [7.8-10.3] σ = 0.7 n = 24 | \bar{x} = 8.6 [7.0-10.2] σ = 0.9 n = 12 | \bar{x} = 7.6 [6.0-9.4] σ = 0.7 n = 132 |
| | MD | 9.1 | 8.6 | \bar{x} = 8.4 [8.0-8.9] σ = 0.4 n = 4 | \bar{x} = 7.6 [6.7-8.7] σ = 0.5 n = 11 | \bar{x} = 7.8 [7.2-8.4] σ = 0.9 n = 2 | \bar{x} = 8.0 [6.9-9.0] σ = 0.5 n = 22 | \bar{x} = 8.2 [6.4-10.0] σ = 1.0 n = 10 | \bar{x} = 6.8 [5.4-8.1] σ = 0.5 n = 124 |
| | RL | -- | 20.6 | -- | \bar{x} = 20.8 - n = 1 | -- | \bar{x} = 20.7 [16.1-25.6] σ = 3.0 n = 16 | \bar{x} = 17.8 [16.1-19.8] σ = 1.3 n = 6 | \bar{x} = 16.6 [13.2-19.2] σ = 1.8 n = 23 |
| P ₃ | BL | 10.2 | 9.6 | \bar{x} = 10.3 [8.9-11.5] σ = 0.9 n = 11 | \bar{x} = 9.0 [8.4-10.0] σ = 0.3 n = 9 | \bar{x} = 9.7 [9.4-10.0] σ = 0.4 n = 2 | \bar{x} = 9.1 [7.2-10.3] σ = 0.7 n = 34 | \bar{x} = 9.1 [8.0-12.2] σ = 1.2 n = 10 | \bar{x} = 8.0 [6.4-10.2] σ = 0.7 n = 173 |
| | MD | 9.7 | 9.2 | \bar{x} = 8.8 [7.9-9.9] σ = 0.6 n = 11 | \bar{x} = 7.9 [7.4-8.4] σ = 0.3 n = 8 | \bar{x} = 9.4 [8.8-10.0] σ = 0.9 n = 2 | \bar{x} = 8.0 [6.3-9.9] σ = 0.7 n = 34 | \bar{x} = 8.2 [7.2-11.0] σ = 1.1 n = 9 | \bar{x} = 7.1 [5.8-8.6] σ = 0.6 n = 160 |
| P ₄ | BL | 10.5 | 10.5 | \bar{x} = 10.6 [9.6-11.7] σ = 0.7 n = 12 | \bar{x} = 8.6 [7.2-10.1] σ = 0.9 n = 11 | \bar{x} = 9.9 [8.7-11.1] σ = 0.9 n = 5 | \bar{x} = 9.3 [7.6-11.1] σ = 0.8 n = 28 | \bar{x} = 9.3 [7.8-10.9] σ = 0.9 n = 16 | \bar{x} = 8.4 [6.8-10.8] σ = 0.7 n = 165 |
| | MD | 9.5 | 8.9 | \bar{x} = 8.7 [7.2-9.9] σ = 0.8 n = 9 | \bar{x} = 7.4 [6.6-9.5] σ = 0.8 n = 11 | \bar{x} = 8.9 [7.5-10.3] σ = 0.9 n = 6 | \bar{x} = 7.9 [5.7-11.8] σ = 1.2 n = 23 | \bar{x} = 7.8 [7.0-9.6] σ = 0.9 n = 12 | \bar{x} = 7.2 [5.6-10.4] σ = 0.7 n = 151 |
| M ₁ | BL | 12.3 | 12.2 | \bar{x} = 12.2 [10.7-13.5] σ = 0.8 n = 15 | \bar{x} = 10.6 [9.7-11.5] σ = 0.6 n = 15 | \bar{x} = 11.7 [10.5-12.6] σ = 0.7 n = 7 | \bar{x} = 11.1 [9.7-12.9] σ = 0.7 n = 37 | \bar{x} = 11.7 [10.5-14.3] σ = 1.0 n = 19 | \bar{x} = 10.7 [8.6-12.6] σ = 0.7 n = 267 |
| | MD | 14.5 | 12.5 | \bar{x} = 13.3 [12.1-14.9] σ = 1.0 n = 13 | \bar{x} = 11.2 [10.6-12.0] σ = 0.5 n = 16 | \bar{x} = 12.8 [11.9-13.8] σ = 0.7 n = 8 | \bar{x} = 11.8 [10.1-13.6] σ = 0.9 n = 34 | \bar{x} = 12.6 [10.8-14.2] σ = 1.0 n = 20 | \bar{x} = 11.4 [9.2-13.5] σ = 0.7 n = 243 |
| M ₂ | BL | 12.2 | 12.2 | \bar{x} = 13.1 [11.7-14.3] σ = 0.8 n = 14 | \bar{x} = 10.4 [8.6-12.4] σ = 0.9 n = 17 | \bar{x} = 11.5 [10.3-12.9] σ = 0.9 n = 6 | \bar{x} = 11.1 [9.6-12.4] σ = 0.7 n = 34 | \bar{x} = 11.0 [9.2-12.7] σ = 1.0 n = 22 | \bar{x} = 10.4 [8.6-12.5] σ = 0.8 n = 207 |
| | MD | (15.3) | 13.0 | \bar{x} = 13.3 [12.5-14.4] σ = 0.6 n = 12 | \bar{x} = 11.5 [9.7-14.8] σ = 1.3 n = 17 | \bar{x} = 12.8 [12.0-13.8] σ = 0.7 n = 6 | \bar{x} = 12.0 [10.5-14.0] σ = 0.9 n = 31 | \bar{x} = 11.7 [10.2-14.2] σ = 1.1 n = 15 | \bar{x} = 10.9 [8.9-14.3] σ = 0.9 n = 198 |
| M ₃ | BL | -- | 11.1 | \bar{x} = 12.4 [11.0-14.2] σ = 0.9 n = 7 | \bar{x} = 10 [8.7-11.3] σ = 0.8 n = 10 | \bar{x} = 11.4 [10.6-12.3] σ = 0.6 n = 5 | \bar{x} = 10.8 [7.9-13.1] σ = 0.8 n = 29 | \bar{x} = 10.8 [9.2-12.8] σ = 1.0 n = 14 | \bar{x} = 10.4 [8.6-12.6] σ = 0.8 n = 139 |
| | MD | -- | 12.8 | \bar{x} = 12.8 [10.9-14.7] σ = 1.3 n = 6 | \bar{x} = 11.2 [9.4-12.7] σ = 0.9 n = 10 | \bar{x} = 13.3 [12.3-15.2] σ = 1.3 n = 4 | \bar{x} = 11.8 [9.4-13.9] σ = 0.9 n = 26 | \bar{x} = 11.8 [10.1-13.8] σ = 1.1 n = 14 | \bar{x} = 10.8 [8.2-12.6] σ = 1.0 n = 119 |

Teeth are identified by letters: C, canine; I, incisor; M, molar; P, premolar. BL, bucco-lingual width; MD, mesiodistal length; RL, root length. All values are in mm. \bar{x} is the mean; minimum and maximum values are between square brackets; σ is the standard deviation; n indicates sample size. Values in parentheses represent uncorrected measurements on worn or cracked teeth. Data sources and sample compositions are in the Methods.

Extended Data Table 5 | Morphological dental trait comparison

| Lower Dentition | Irhoud 3, 11 | <i>H. erectus</i> | MPE | MPAf | Neanderthals | EMH | RMH |
|---|-----------------|-------------------|----------|----------|--------------|-----------|------------|
| P ₄ Lingual Cusps [pres. >1] | 50 (2) | 85.7 (7) | 66.7 (3) | 75 (4) | 93.9 (33) | 75 (8) | 66.7 (173) |
| P ₄ Metaconid position [pres. = mesial] | 100 (2) | 90.9 (11) | 100 (4) | 75 (4) | 100 (34) | 66.7(9) | 80.6 (177) |
| P ₄ Transverse Crest [pres. >0] | 0 (2) | 36.4 (11) | 25 (4) | 83.3 (6) | 75.8 (33) | 11.1 (9) | 4.5 (177) |
| P ₄ Distal Accessory Ridge [pres. >0] | 50 (2) | 75 (8) | 100 (2) | 66.7 (3) | 82.4 (17) | 50 (4) | 47.1 (145) |
| P ₄ Mesial Accessory Ridge [pres. >0] | 0 (2) | 0 (7) | 33.3 (3) | 66.7 (3) | 10.5 (19) | 75 (4) | 29.5 (152) |
| P ₄ Asymmetry [pres. >0] | 100 (2) | 46.2 (13) | 0 (4) | 50 (4) | 94.3 (35) | 20 (10) | 0.8 (119) |
| P ₄ Fissure Pattern [pres. = U] | 0 (2) | 0 (5) | 0 (2) | 0 (2) | 0 (29) | 75 (4) | 72.9 (145) |
| M ₁ Middle Trigonid Crest [pres. >0] | 0 (2) | 33.3 (12) | 85.7 (9) | 50 (2) | 94.9 (39) | 35.7 (14) | 1.4 (207) |
| M ₁ Protostylid [pres.>2] | 50 (2) | 50 (8) | 0 (7) | 33.3 (3) | 0 (43) | 12.5 (16) | 0.5 (218) |
| M ₁ Cusp 6 [pres. >0] | 100 (2) | 28.6 (7) | 40 (5) | 100 (1) | 32 (25) | 0 (14) | 18.1 (200) |
| M ₁ Cusp 7 [pres. >0] | 100 (2) | 50 (12) | 0 (6) | 0 (2) | 30 (40) | 42.9 (21) | 9.7 (236) |
| M ₂ Y Groove Pattern [pres. = Y] | 50 (2) | 91.7 (12) | 80 (5) | 0 (2) | 69.2 (39) | 68.8 (16) | 28.6 (242) |
| M ₂ Cusp number [pres.= 4] | 0 (2) | 0 (13) | 0 (5) | 0 (5) | 2.4 (42) | 15 (20) | 63.8 (242) |

| Upper Dentition | Irhoud 10, 21, 22 | <i>H. erectus</i> | MPE | MPAf | Neanderthals | EMH | RMH |
|--|----------------------|-------------------|----------|---------|--------------|----------|------------|
| I ² Shoveling [pres >1] | Present (1) | 100 (3) | -- | 100 (1) | 100 (29) | 83.3 (6) | 23.2 (122) |
| I ² Tuberculum dentale [pres. >1] | Present (1) | 0 (2) | -- | 100 (1) | 95.5 (22) | 60 (5) | 38.1 (118) |
| C Distal Accessory Ridge [pres. >0] | Present (1) | 66.7 (3) | -- | 100 (1) | 46.7 (15) | 100 (2) | 39.7 (68) |
| M ¹ Cusp 5 [pres. >0] | Present (1) | 0 (2) | 67.7 (3) | 100 (1) | 57.7 (26) | 50 (10) | 41.2 (232) |
| M ¹ Carabelli's Trait [pres. >2] | | 0 (2) | 33.3 (3) | 0 (1) | 71.4 (28) | 50 (10) | 46.2 (272) |
| M ¹ Parastyle [pres. >0] | Absent (2) | 0 (1) | 0 (2) | 0 (1) | 20 (25) | 0 (14) | 0.8 (299) |
| M ¹ Mesial Accessory Cusps [pres >0] | Absent (1) | -- | 0 (2) | -- | 50 (14) | 100 (2) | 67.1 (132) |
| M ² Metacone Reduction [pres. <3.5] | 0 (2) | 0 (8) | 0 (4) | 0 (4) | 2.9 (35) | 0 (10) | 18.3 (243) |
| M ² Hypocone Reduction [pres. <3] | 0 (2) | 0 (8) | 0 (4) | 0 (7) | 2.9 (35) | 0 (8) | 24.5 (241) |

Teeth are identified by letters: C, canine; I, incisor; M, molar; P, premolar. Numbers given are trait frequency scores at the enamel surface. Pres., present. Sample sizes are in brackets. Data sources and sample compositions are in the Methods.